

# Constitutive Models To Describe The Response of Materials For High Temperature Operating Conditions

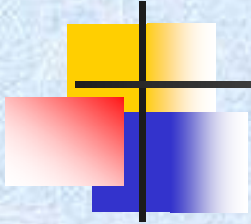
---

K. R. Rajagopal  
Texas A&M University

I. Joga Rao  
New Jersey Institute of Technology

Grant # DE-FG26-06NT42714

# Outline



- Introduction
- Overview of creep in Ni based superalloys
- Development of constitutive equations
- Results



# Introduction

---

Objective: To develop constitutive models for materials operating at high temperatures: modern single crystal superalloys

- The model development will lead to better predictive capability of the response of single crystal turbine blades
- Better creep characteristics of single crystal superalloys will lead to enhanced efficiency of gas turbines



# Introduction

---

- Higher inlet temperature → higher efficiency, low fuel costs
- Last 3 decades – turbine airfoil temperature capacity has increased on an average by 4 °F per year
- Contribution to the increased temperature capacity  
~ 40 % due to advanced materials (single crystal superalloys)

# Introduction

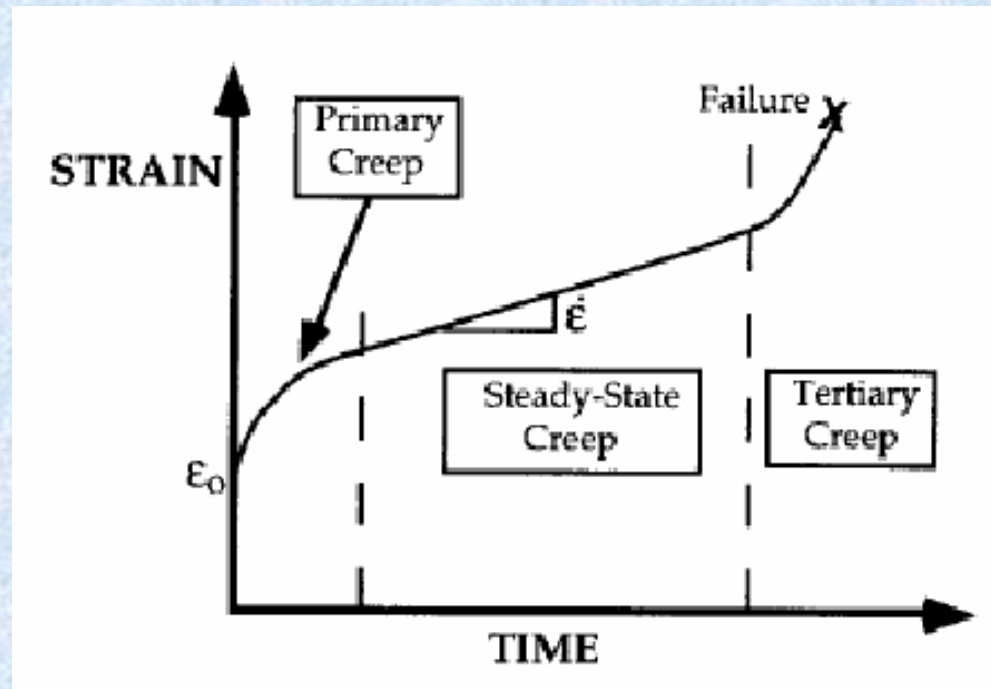


---

- Single crystal superalloys have complex thermo-mechanical response
  - Modeling the response of such materials
  - It is expected that a constitutive model will
    - optimize the efficiency in design of components w.r.t preventing failure and preventing over design
    - eliminate the need for performing specimen tests for all component conditions (Huge savings in terms of cost and time!)

# A Typical Creep Curve

- Stages of Creep



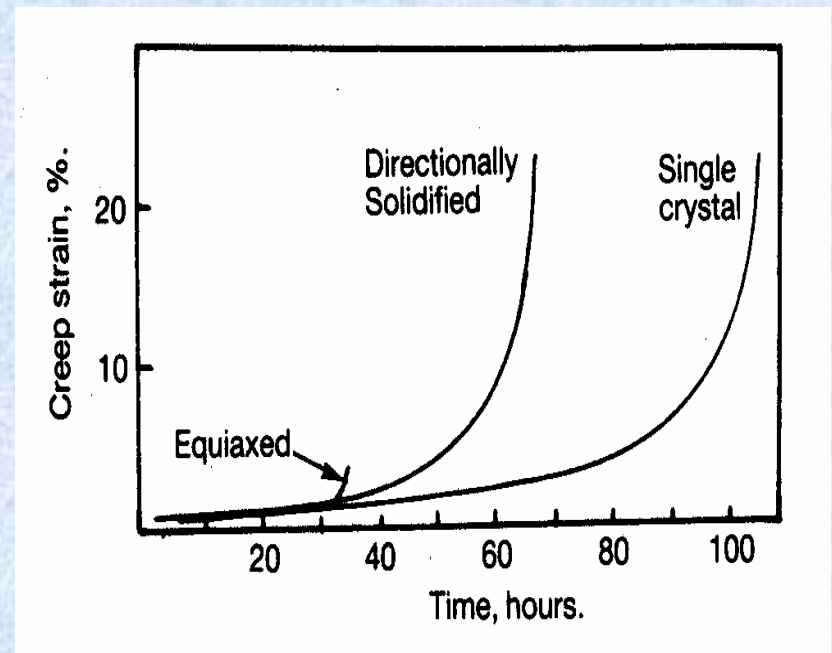
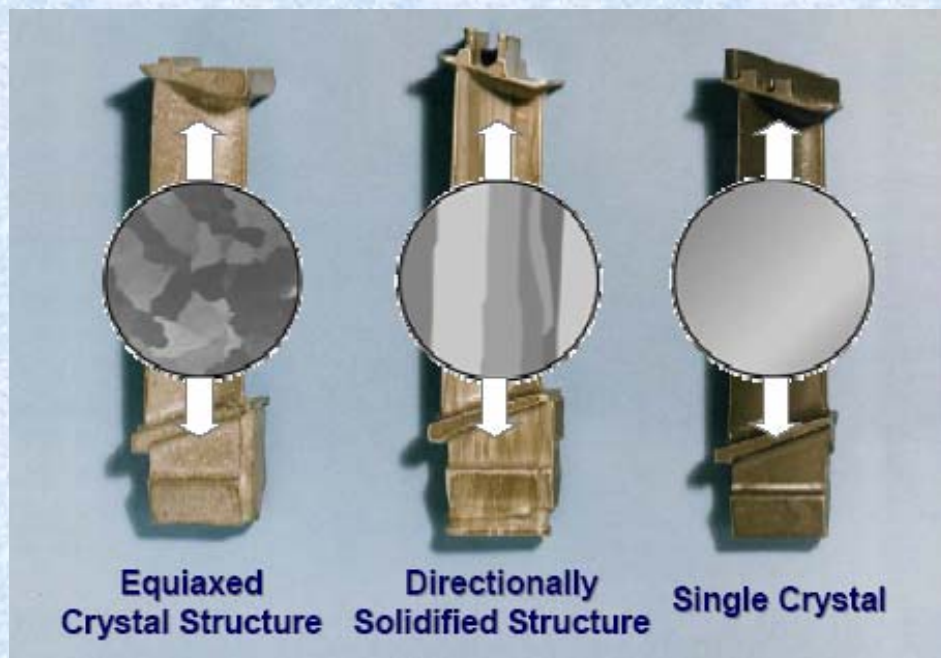
A typical creep curve

# Creep of Nickel Superalloys

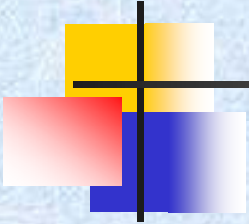
## Relationship to Microstructure

### 1. Characteristics of creep

a. Single crystal has the longest creep life



# Factors Affecting Creep

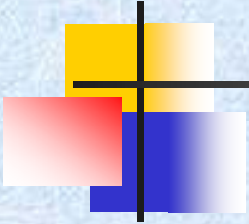


## 2. Factors that affect the creep life

- a.  $\gamma'$  volume and size
- b. Misfit
- c. Rafting
- d. Orientation
- e. Temperature and stress



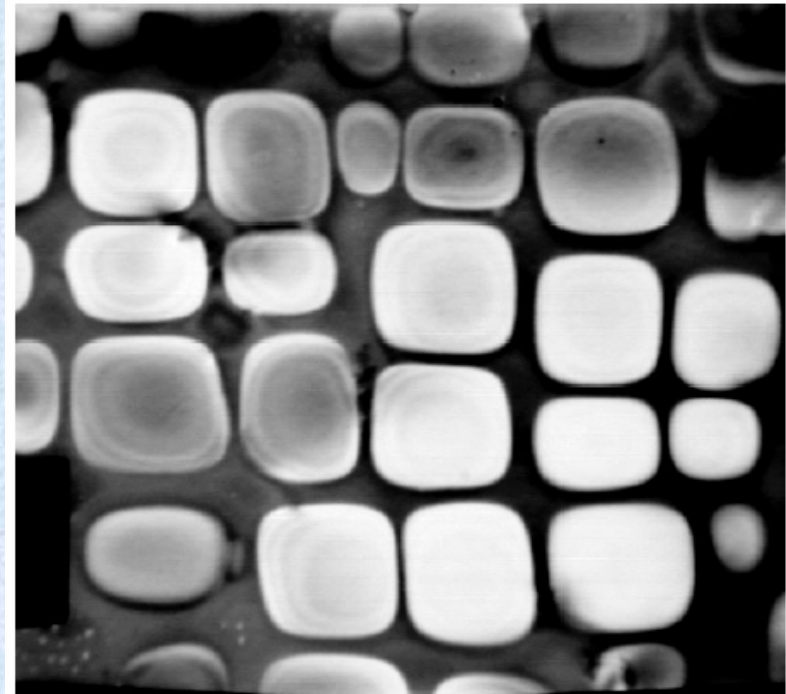
# Microstructure of Nickel Based Single Crystal Superalloy



$\gamma'$  volume and size

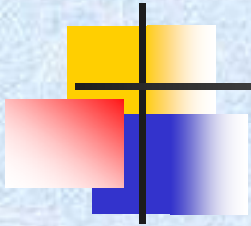
Peak value: 70-80%

Size: 0.4-0.5  $\mu$  m

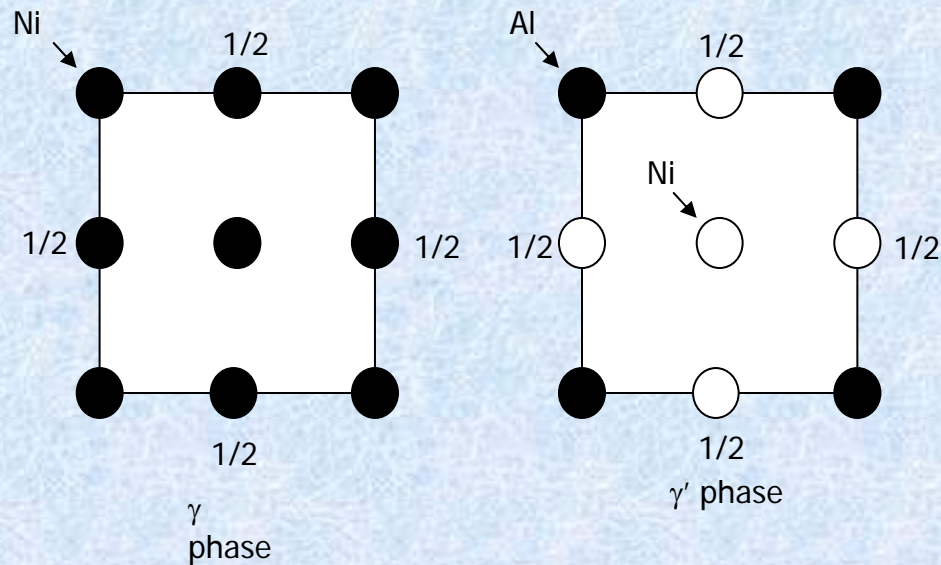


TEM photography of Nickel based single crystal superalloy SC16

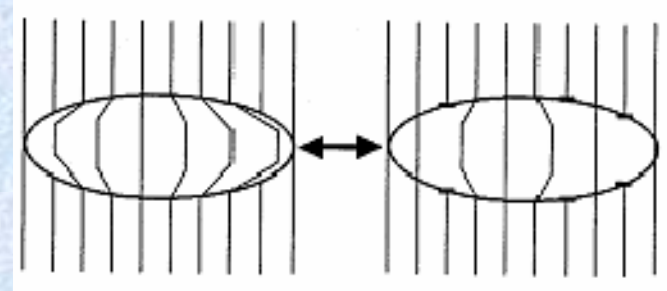
# Microstructure of Nickel Based Single Crystal Superalloy



Lattice misfit



$\gamma$  and  $\gamma'$  cell projections

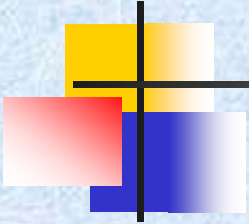


coherence incoherence

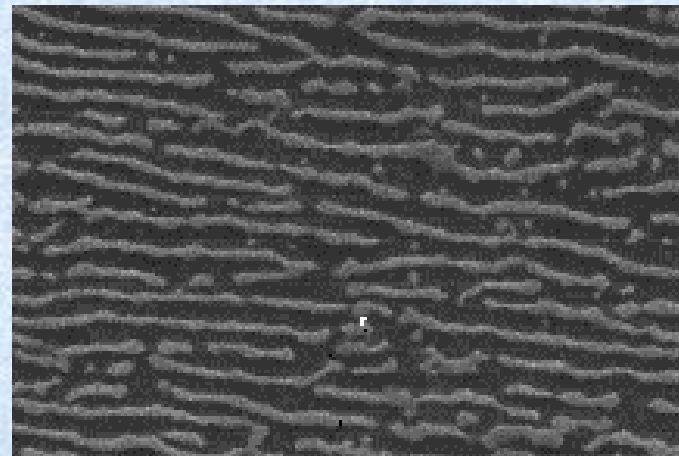
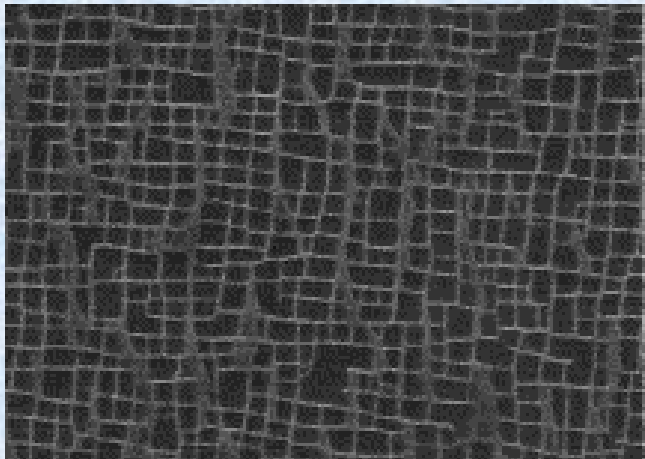
Schematic plot of coherence

Maximum creep rupture life when the misfit is a small fraction of 1% and when volume fraction of  $\gamma'$  is as high as possible. (Decreasing the misfit from 0.2% to zero led to a 50x increase in creep rupture life!)

# Directional Coarsening of $\gamma'$



## 3. Rafting: directional coarsening of $\gamma'$

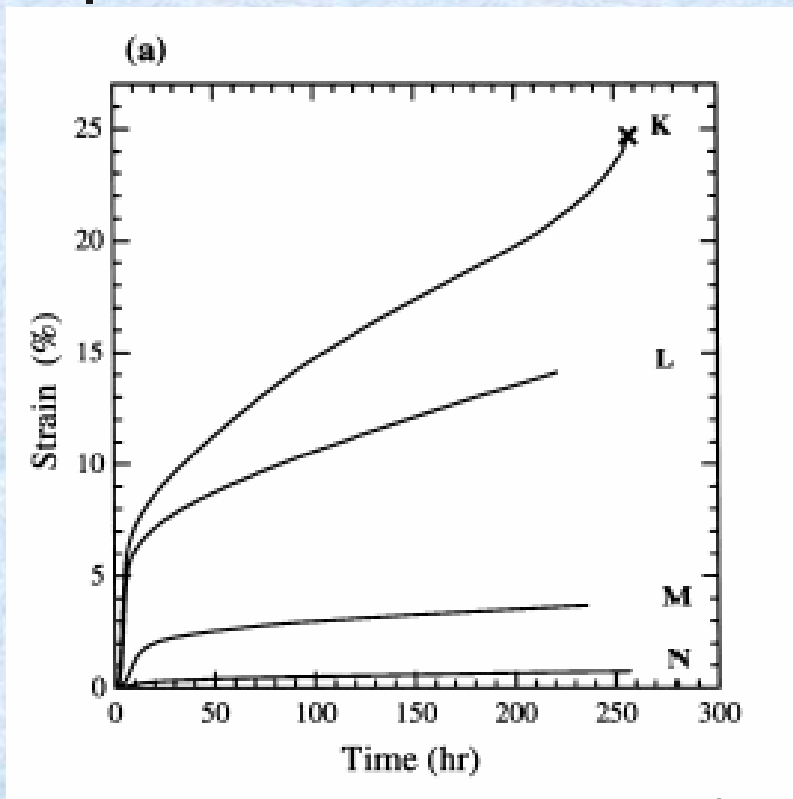


Microstructure changes during creep

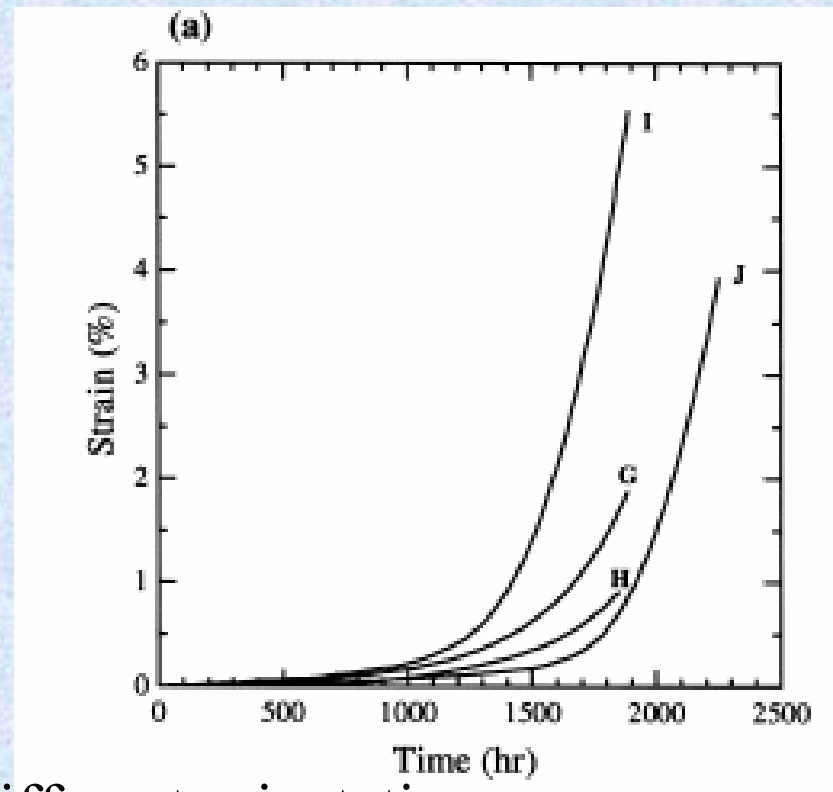
The  $\gamma'$  precipitates coarsen (Ostwald ripening) very slowly, because of the low interfacial energy between the  $\gamma$  and  $\gamma'$

# Anisotropic Creep

Creep is highly anisotropic



750 °C

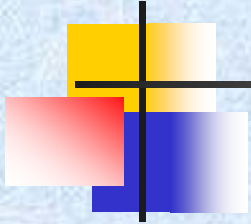


950 °C

Creep for different orientations

From Matan et al. (1999)

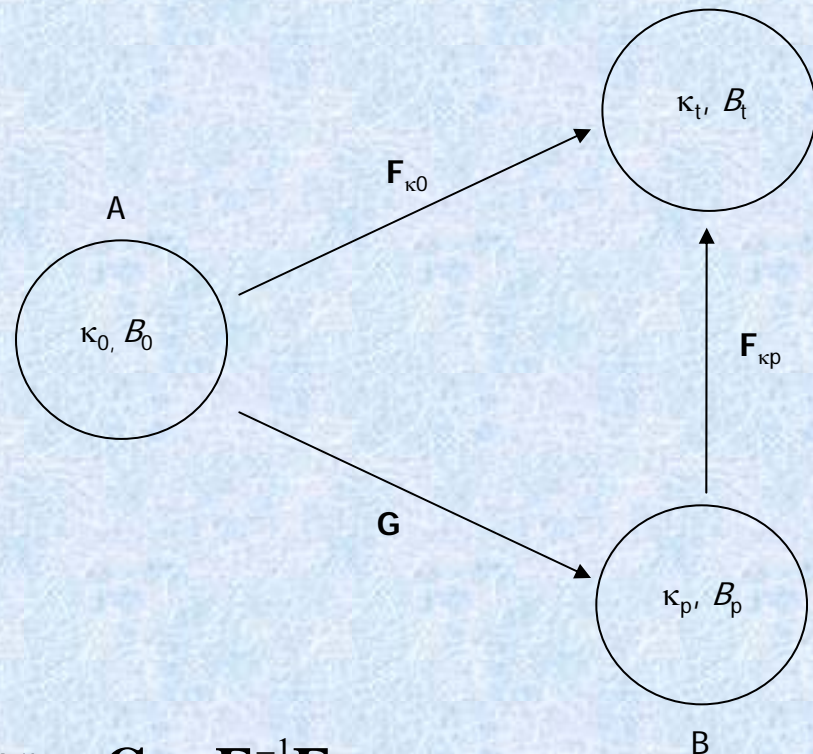
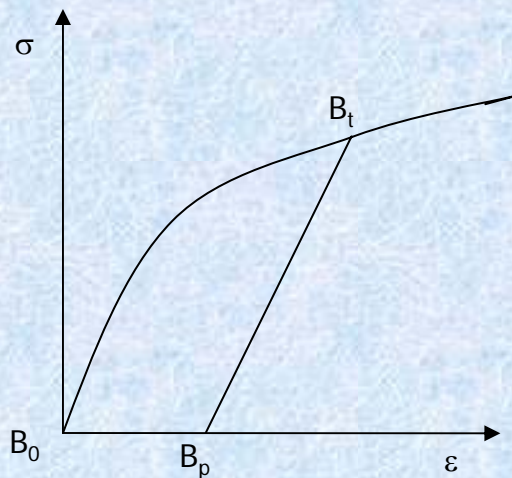
# Development of Constitutive Equations



- Use the theory of multiple natural configurations, as a crystal can exist stress free in more than one configuration.
- Develop a consistent thermodynamic setting, utilizing the maximization of rate of dissipation to obtain evolution equations for the natural configurations.
- Incorporate main features described: Anisotropy, Temperature dependence and microstructural effects, in an averaged manner.

# Multiple Natural Configurations

- A body can possess many natural configurations;
- Response is elastic from these configurations.
- Evolution of underlying natural configuration has to be prescribed.

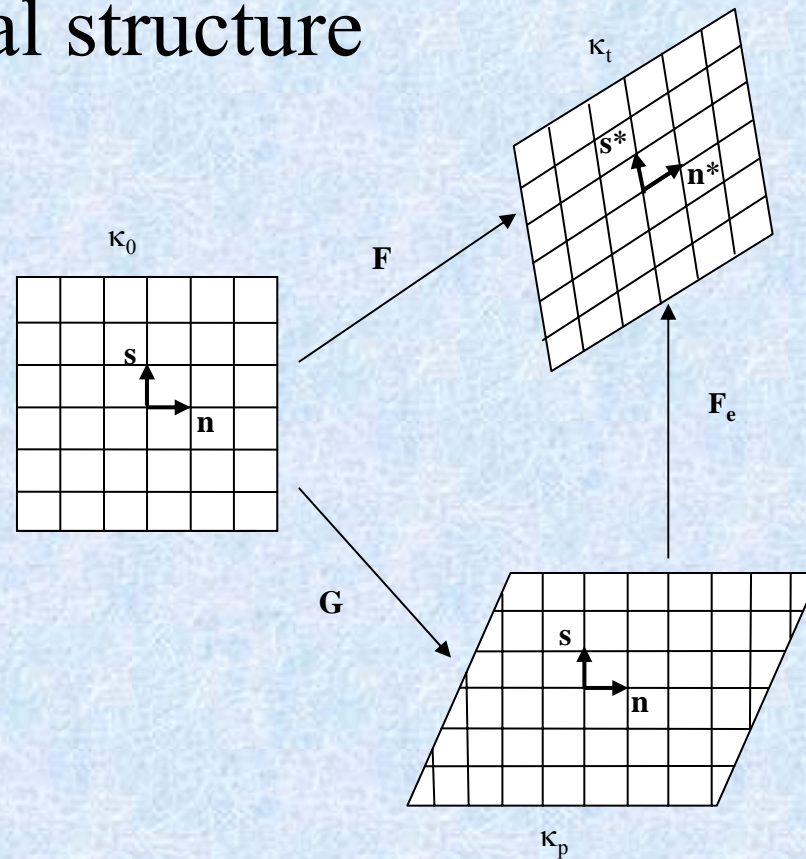


Evolution of the natural configuration

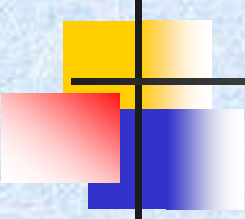
$$\mathbf{G} = \mathbf{F}_{\kappa_p}^{-1} \mathbf{F}_{\kappa_0}$$

# Natural configurations associated with single crystals

- Anisotropy associated with underlying crystal structure



# Model Development

- 
- Second Law (Reduced Energy Dissipation Equation)

$$\mathbf{T} \cdot \mathbf{L} - \rho \dot{\psi} - \rho \eta \dot{\theta} - \frac{\mathbf{q} \cdot \text{grad} \theta}{\theta} = \rho \theta \xi := \zeta \geq 0$$

- After Simplification

$$\mathbf{T} \cdot \mathbf{L} - \rho \dot{\psi} = \zeta_{mech} \geq 0$$

- Need to prescribe constitutive equations for the:
  - Stored Energy  $\psi$
  - Rate of Dissipation  $\zeta$



# Model Development

- Stored Energy

$$\psi = \psi(\mathbf{F}_e, \mathbf{G})$$

- On Simplification, stress is obtained as

$$\mathbf{T} = 2\rho\mathbf{F}_e \frac{\partial\psi}{\partial\mathbf{C}_e} \mathbf{F}_e^T$$

- Second Law reduces to

$$\mathbf{A} \cdot \mathbf{D}_p + \boldsymbol{\tau} \cdot \mathbf{W}_p - \rho \frac{d\tilde{\psi}}{dt} = \zeta_{mech} \geq 0,$$

$$\mathbf{A} = (\mathbf{F}_e^T \mathbf{T} \mathbf{F}_e^{-T})_{sym} \quad \boldsymbol{\tau} = (\mathbf{F}_e^T \mathbf{T} \mathbf{F}_e^{-T})_{skew}$$



# Specific Forms for Stored Energy

- Total stored energy is split:

$$\psi = \hat{\psi}(\mathbf{F}_e) + \tilde{\psi}(\mathbf{G})$$

- Elastic Part

$$\hat{\psi} = \frac{1}{\rho} \mathbf{E}_e \cdot \mathbf{C} \mathbf{E}_e$$

$$\mathbf{C} = \begin{pmatrix} c_{11} & c_{12} & c_{12} & 0 & 0 & 0 \\ c_{12} & c_{11} & c_{12} & 0 & 0 & 0 \\ c_{12} & c_{12} & c_{11} & 0 & 0 & 0 \\ 0 & 0 & 0 & c_{44} & 0 & 0 \\ 0 & 0 & 0 & 0 & c_{44} & 0 \\ 0 & 0 & 0 & 0 & 0 & c_{44} \end{pmatrix}$$

Fourth order elasticity tensor for a FCC crystal

# Inelastic Stored Energy

- Two main energy storage mechanisms (Mollica, Srinivasa and Rajagopal (2001))
- Energy stored in dislocation networks
- Use a dislocation density  $a(s)$  that depends on the inelastic strain path length,  $s$

$$\dot{s} = \|\mathbf{D}_p\|; \quad s = \int_0^t \|\mathbf{D}_p\| d\tau$$

$$a(s) = a_o \left( 1 + \beta_2 \left( 1 - e^{-\alpha_1 s} \right) \right)$$

- Based on experimental observations:
  - Dislocation density increases with inelastic deformation.
  - It reaches a saturation point.

# Inelastic Stored Energy (contd)

- Second storage mechanism is due to the presence of the second hard  $\gamma'$  phase.
- Dislocations face significant resistance to their motion.
- In particular they can get pinned
- Based on the work of Mollica et al. (2001)

$$\tilde{\psi} = \underbrace{\psi_1 a(s)}_{\text{Dislocation Networks}} + \underbrace{\psi_2 \int_0^s e^{\eta(x-s)} (\mathbf{E}_p(s) - \mathbf{E}_p(x)) \bullet \mathbf{N}(x) dx}_{\text{Resistance due to second phase}}$$

Dislocation  
Networks

Resistance due  
to second phase



## Inelastic Stored Energy (contd)

$$\rho \frac{d\tilde{\psi}}{dt} = h(s)(\mathbf{D}_p \cdot \mathbf{D}_p)^{\frac{1}{2}} + \boldsymbol{\alpha} \cdot \mathbf{D}_p,$$

$$\boldsymbol{\alpha} = \rho \psi_2 \int_0^s e^{\eta(x-s)} \mathbf{N}(x) dx, \quad \mathbf{N} = \frac{\mathbf{D}_p}{\sqrt{\mathbf{D}_p \cdot \mathbf{D}_p}}$$

$$h(s) := \rho [\psi_1 (a' + \eta a) - \eta \tilde{\psi}], \text{ Hardening}$$

$$\dot{\boldsymbol{\alpha}} = \rho \psi_2 \mathbf{D}_p - \eta (\mathbf{D}_p \cdot \mathbf{D}_p)^{\frac{1}{2}} \boldsymbol{\alpha}$$

- Generalized version of non-linear kinematic hardening rule
- Equation for Backstress falls out naturally from our choice of inelastic stored energy !
- No ad hoc prescription of backstress !



# Structure of Rate of Dissipation

$$\zeta_1 = \mathbf{D}_p \cdot \mathbf{K} \mathbf{D}_p,$$

- Need to prescribe the fourth order tensor  $\mathbf{K}$
- Dissipation is due to two main reasons:
- Movement of mobile dislocations
  - $\mathbf{K}$  depends on the density of mobile dislocations
  - According to Gilman (1969)  
Mobile dislocations =  $a(s)e^{-\alpha_2 s}$
- Softening due to cavitation in the latter stages of creep.

# Rate of Energy Storage

$$\frac{\mathbf{T.L}}{\rho} = \rho\dot{\psi} + \zeta_{mech}$$
$$\underbrace{\quad}_{W_t} = \underbrace{\quad}_{W_s} + \underbrace{\quad}_{W_d}$$

Total Work Done=Work Stored + Work Dissipated

- Each work term arises naturally because of the thermodynamic framework used.
- No ad-hoc coefficients used.
- Instantaneous rate of energy storage,  $R$

$$R = 1 - \frac{W_d}{W_T} = \frac{W_s}{W}$$

# Constitutive Model

- Maximization of Rate of Dissipation to determine
$$\mathbf{L}_p = \mathbf{D}_p + \mathbf{W}_p$$
- Note: Evolution of natural configuration depends on the driving force

$$\mathbf{A} = p\mathbf{I} + \mathbf{A}^*,$$

$$\mathbf{A}^* = \alpha + \mathbf{K}\mathbf{D}_p + h(s) \frac{\mathbf{D}_p}{(\mathbf{D}_p \cdot \mathbf{D}_p)^{\frac{1}{2}}},$$

$$p = \frac{1}{3} \text{tr}(\mathbf{A} - \mathbf{A}^*)$$

$$\mathbf{W}_p = \frac{1}{\eta_2} \boldsymbol{\tau}$$



# Results



---

- The initial results that are presented are obtained using MATLAB.
- Later we will discuss the development of UMAT (User Defined Material Subroutine) and the use of Abaqus to solve boundary value problems for more complex geometries for bodies.

# Results

- The problem is solved (for loading along  $\langle 001 \rangle$ ,  $\langle 111 \rangle$  and  $\langle 011 \rangle$ ) assuming homogeneous deformations with a semi-inverse approach

$$\mathbf{F} = \text{diag}(\phi_1(t), \phi_2(t), \phi_3(t))$$

$$\mathbf{F}_e = \text{diag}(\lambda_1, \lambda_2, \lambda_3)$$

$$\mathbf{G} = \text{diag}\left(\frac{\phi_1(t)}{\lambda_1}, \frac{\phi_2(t)}{\lambda_2}, \frac{\phi_3(t)}{\lambda_3}\right)$$

- Governing differential equations are obtained using equations for evolution of natural configurations

# Material Parameters

$\psi_1$  : Proportionality constant for inelastic free energy stored in dislocation networks

$\psi_2$  : Proportionality constant for inelastic free energy due to hardening caused by  $\gamma'$  precipitates

$\eta$  : Parameter which tells how strongly stored energy depends on deformation history

$\beta_2$  : Dislocation multiplication factor

$\alpha_1$  : Parameter which tell how fast dislocation density saturates

$\alpha_2, \Omega_2$  : Attrition coefficient, related to the fraction of dislocations which are mobile

$\alpha_3, \Omega_3$  : Parameter related to dissipation due to damage accumulation

$\kappa_1, \Gamma_1$  : Parameter which tell how the first mechanism of dissipation depends on driving force

$\kappa_2, \Gamma_2$  : Parameter which tell how the second mechanism of dissipation depends on driving force

$\beta_1, \Lambda_1$  : Proportionality constant for first dissipation mechanism

$\beta_3, \Lambda_3$  : Proportionality constant for second dissipation mechanism

- Model corroborated with  $\langle 001 \rangle$  &  $\langle 111 \rangle$  orientations
- 17 Material Parameters (far lesser than crystal plasticity based models)

# Anisotropic Creep Results

## $\langle 001 \rangle$ , $\langle 011 \rangle$ , $\langle 111 \rangle$ directions

- Loading axis can be in an arbitrary direction.
- Requires mapping quantities back and forth between the global and crystal coordinate system.
- Fourth order tensor  $\mathbf{K}$ .

$$\mathbf{K}^{-1} = \begin{bmatrix} i & j & j & 0 & 0 & 0 \\ j & i & j & 0 & 0 & 0 \\ j & j & i & 0 & 0 & 0 \\ 0 & 0 & 0 & k & 0 & 0 \\ 0 & 0 & 0 & 0 & k & 0 \\ 0 & 0 & 0 & 0 & 0 & k \end{bmatrix}$$

## Anisotropic Creep, 800°C, <001>, (CMSX-4)

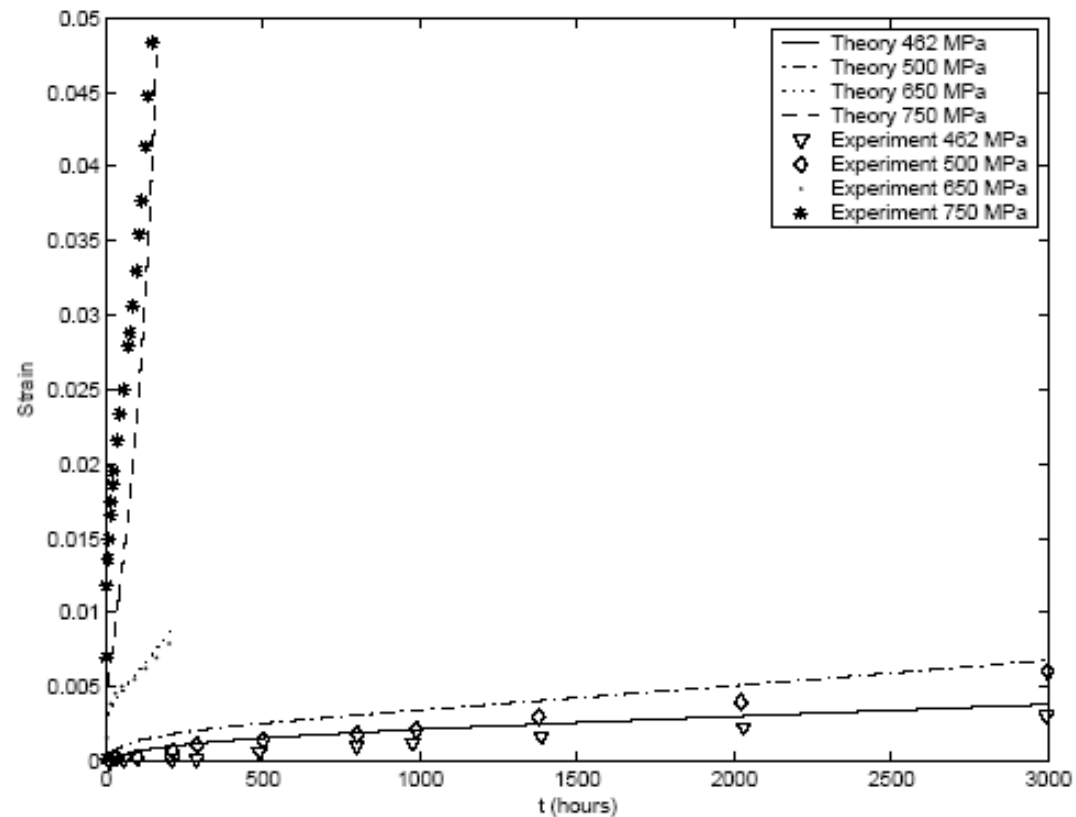


Figure 2: Strain vs. time for CMSX-4 for loading along the <001> orientation,  $\theta = 800\text{ }^{\circ}\text{C}$ : Comparison of the predictions of the model with experimental results of Schubert et al., [24].

## Anisotropic Creep, 800°C, <111>, (CMSX-4)

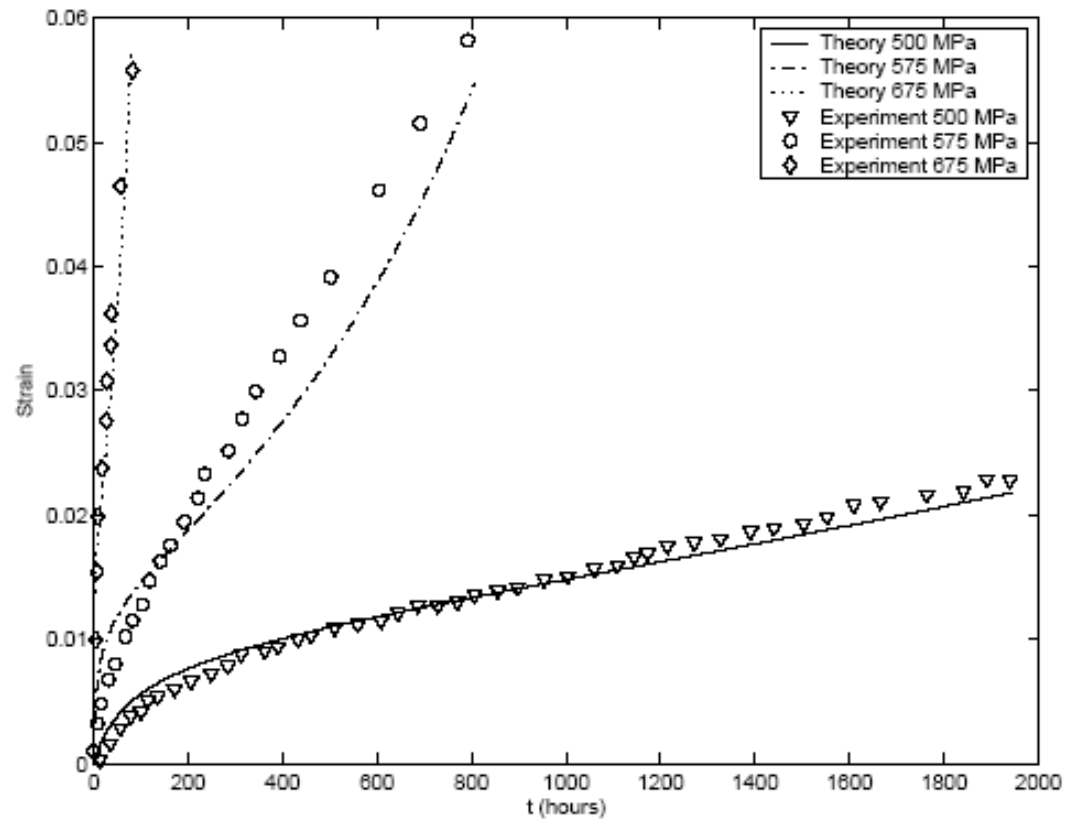


Figure 3: Strain vs. time for CMSX-4 for loading along the <111> orientation,  $\theta = 800$  °C: Comparison of the predictions of the model with experimental results of Schubert et al., [24].

## Anisotropic Creep, 800°C, <011>, (CMSX-4)

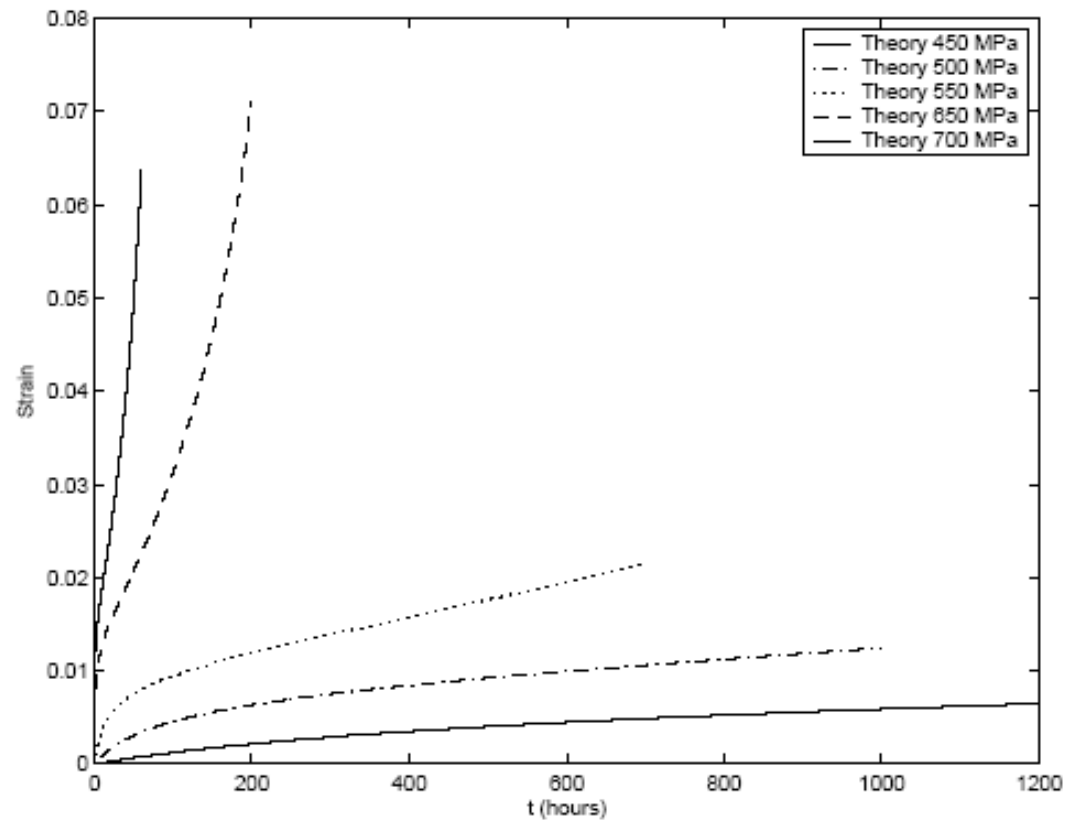


Figure 4: Strain vs. time for CMSX-4 for loading along the <011> orientation,  $\theta = 800$  °C.

Predictions of the model !!

## Anisotropic Creep, 950°C, <001>, (CMSX-4)

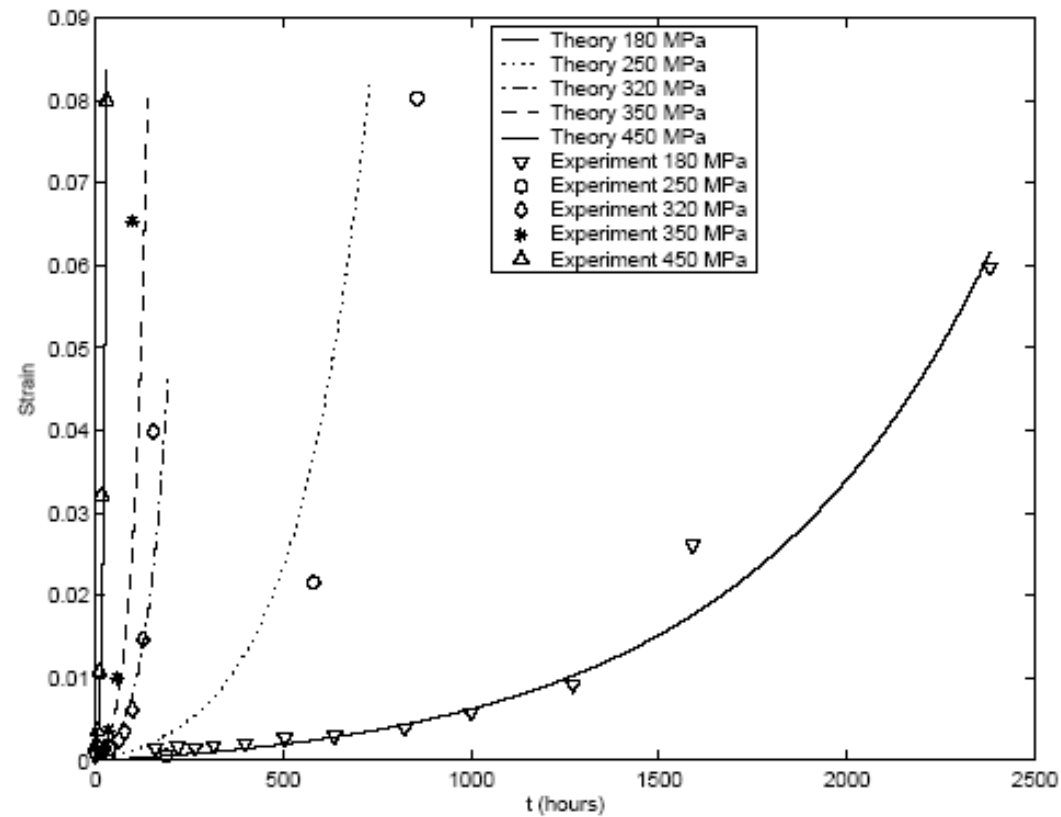


Figure 5: Strain vs. time for CMSX-4 for loading along the <001> orientation,  $\theta = 950$  °C: Comparison of the predictions of the model with experimental results of MacLachlan et al., [25].



## Anisotropic Creep, 950°C, <111>, (CMSX-4)

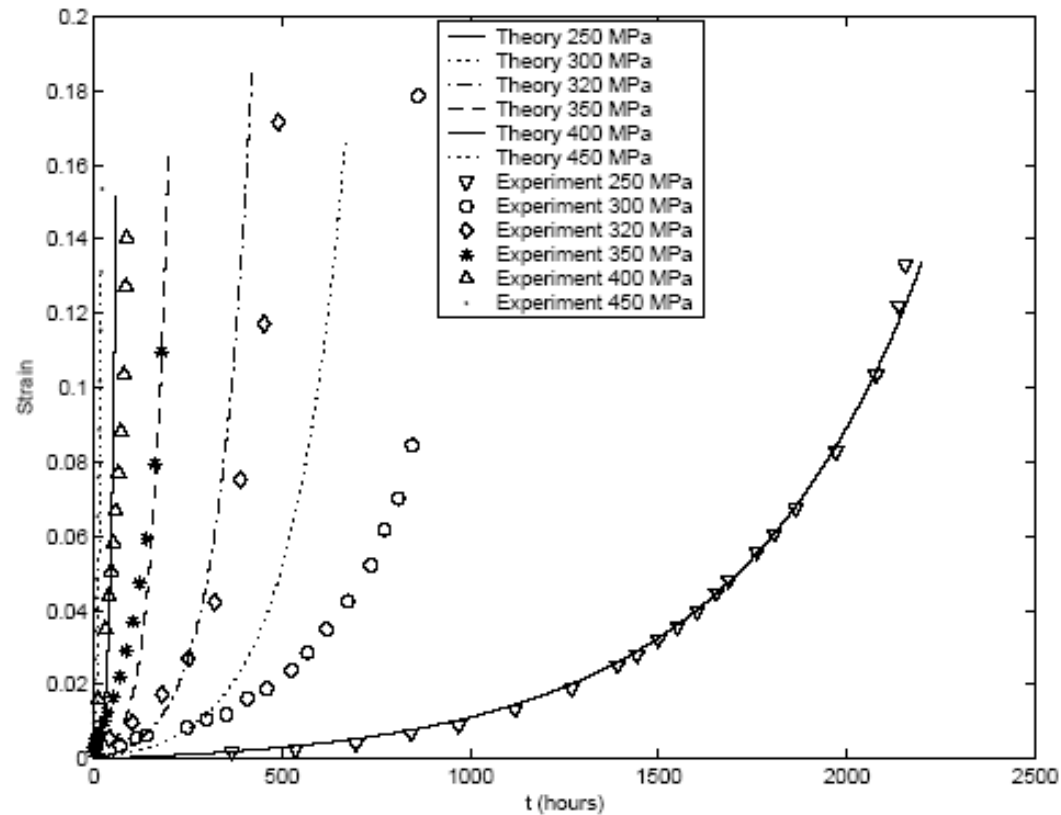


Figure 6: Strain vs. time for CMSX-4 for loading along the <111> orientation,  $\theta = 950 \text{ }^\circ\text{C}$ : Comparison of the predictions of the model with experimental results of MacLachlan et al., [25].

## Anisotropic Creep, 950°C, <011>, (CMSX-4)

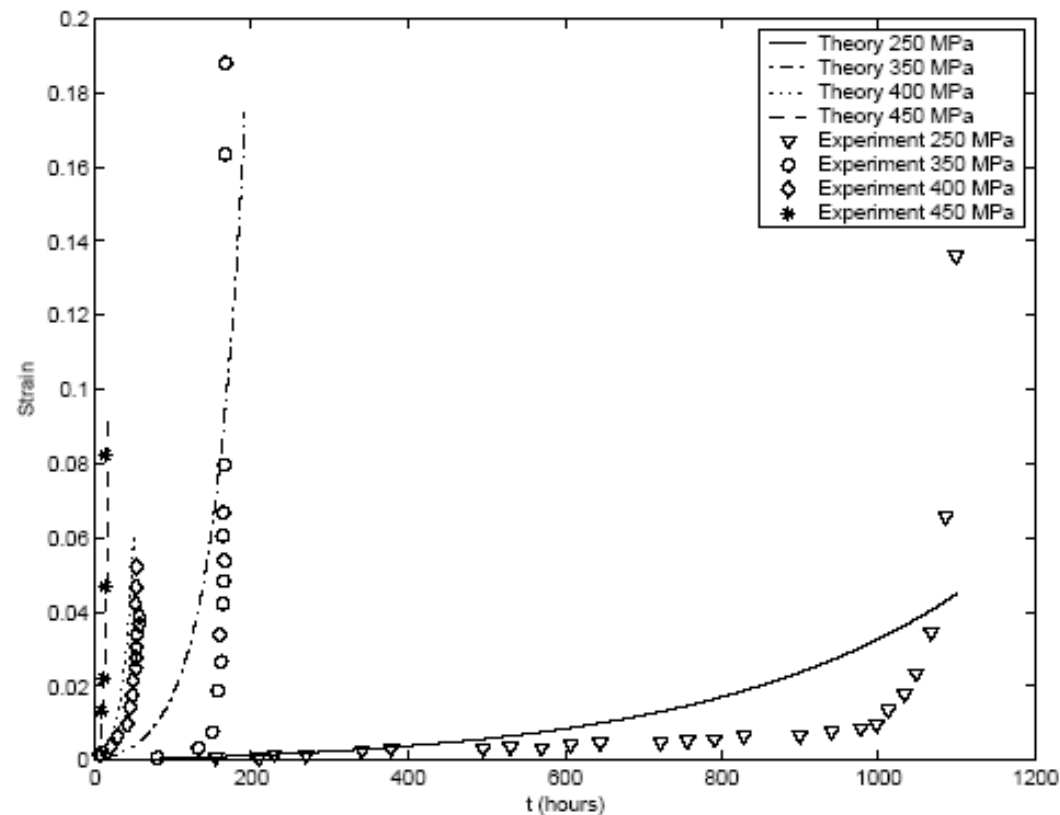
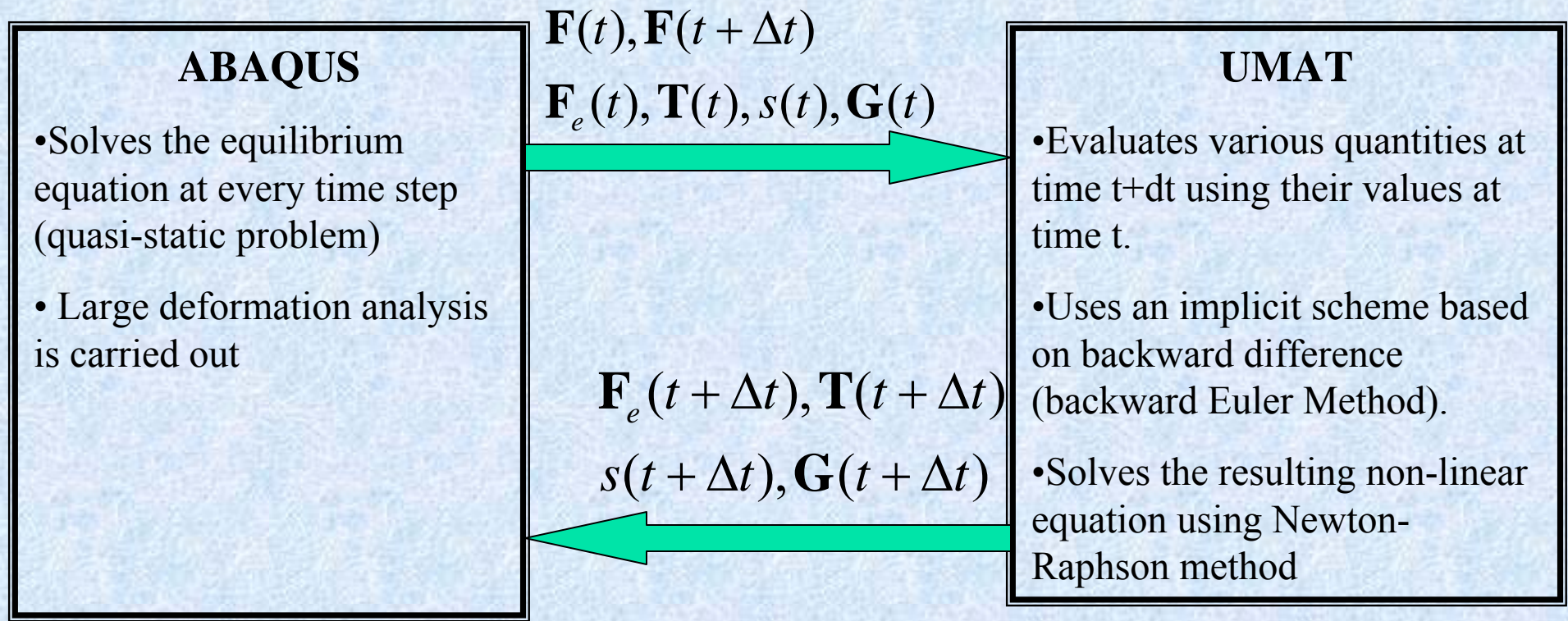


Figure 7: Strain vs. time for CMSX-4 for loading along the <011> orientation,  $\theta = 950$  °C: Comparison of the predictions of the model with experimental results of MacLachlan et al., [25].

Model corroborated with <001> & <111> predicts <011> well !!

# Computational Subroutines in Abaqus

- The constitutive model has been implemented in Abaqus/Standard through UMAT



# Numerical Scheme in UMAT

- Numerical scheme based on first order backward difference (implicit scheme, unconditionally stable)

First Order Backward Difference

$$f_1 := {}^{t+\Delta t} s - {}^t s - \Delta t \sqrt{\left( {}^{t+\Delta t} \mathbf{D}_p \cdot {}^{t+\Delta t} \mathbf{D}_p \right)} = 0$$

$$f_2 := {}^{t+\Delta t} \mathbf{D}_p - \left( {}^{t+\Delta t} \bar{\mathbf{K}} \right)^{-1} \left( {}^{t+\Delta t} \mathbf{A} - \frac{1}{3} \text{tr}({}^{t+\Delta t} \mathbf{A}) \mathbf{1} - {}^{t+\Delta t} \boldsymbol{\alpha} \right) = \mathbf{0}$$

$$f_3 := {}^{t+\Delta t} \boldsymbol{\alpha} - {}^t \boldsymbol{\alpha} - \rho \psi_2 \Delta t {}^{t+\Delta t} \mathbf{D}_p + \eta {}^{t+\Delta t} \boldsymbol{\alpha} \left( {}^{t+\Delta t} s - {}^t s \right) = \mathbf{0}$$

$$f_4 := {}^{t+\Delta t} \tilde{\psi} - {}^t \tilde{\psi} - \frac{h(s)}{\rho} \left( {}^{t+\Delta t} s - {}^t s \right) - \Delta t {}^{t+\Delta t} \boldsymbol{\alpha} \cdot {}^{t+\Delta t} \mathbf{D}_p = 0$$



# Numerical Scheme in UMAT

Need to find solution to  $\mathbf{F}(\mathbf{X}) = \{\mathbf{0}\}$

$$\mathbf{F} = \begin{Bmatrix} f_1 \\ f_2 \\ f_3 \\ f_4 \end{Bmatrix} \quad \mathbf{X} = \begin{Bmatrix} {}^{t+\Delta t} S \\ {}^{t+\Delta t} \mathbf{D}_p \\ {}^{t+\Delta t} \boldsymbol{\alpha} \\ {}^{t+\Delta t} \tilde{\psi} \end{Bmatrix} \quad [\mathbf{J}] = \frac{\partial \mathbf{F}}{\partial \mathbf{X}}$$

Use Newton Raphson Scheme

$$\mathbf{X}^{k+1} = \mathbf{X}^k - [\mathbf{J}]^{-1} \mathbf{F}(\mathbf{X}^k), \quad k - \text{iteration number}$$

Update of  $\mathbf{G}$  (Eterovic and Bathe (1990))

$${}^{t+\Delta t} \mathbf{G} = \exp(\Delta t {}^{t+\Delta t} \mathbf{L}_p) {}^t \mathbf{G}$$

Update on  $\mathbf{F}_e$

$${}^{t+\Delta t} \mathbf{F}_e = {}^{t+\Delta t} \mathbf{F} \left( {}^{t+\Delta t} \mathbf{G} \right)^{-1}$$



# Computational Subroutines in Abaqus

---

- Inelastic strain pathlength  $S$ , and tensor  $\mathbf{G}$  are stored as solution dependent variables (SDV)
- Initial conditions on solution dependent variables (SDV) are imposed through User Routine SDVINI in Abaqus/Standard
- Orientation of crystal lattice is imposed through User Routine ORIENT in Abaqus/Standard

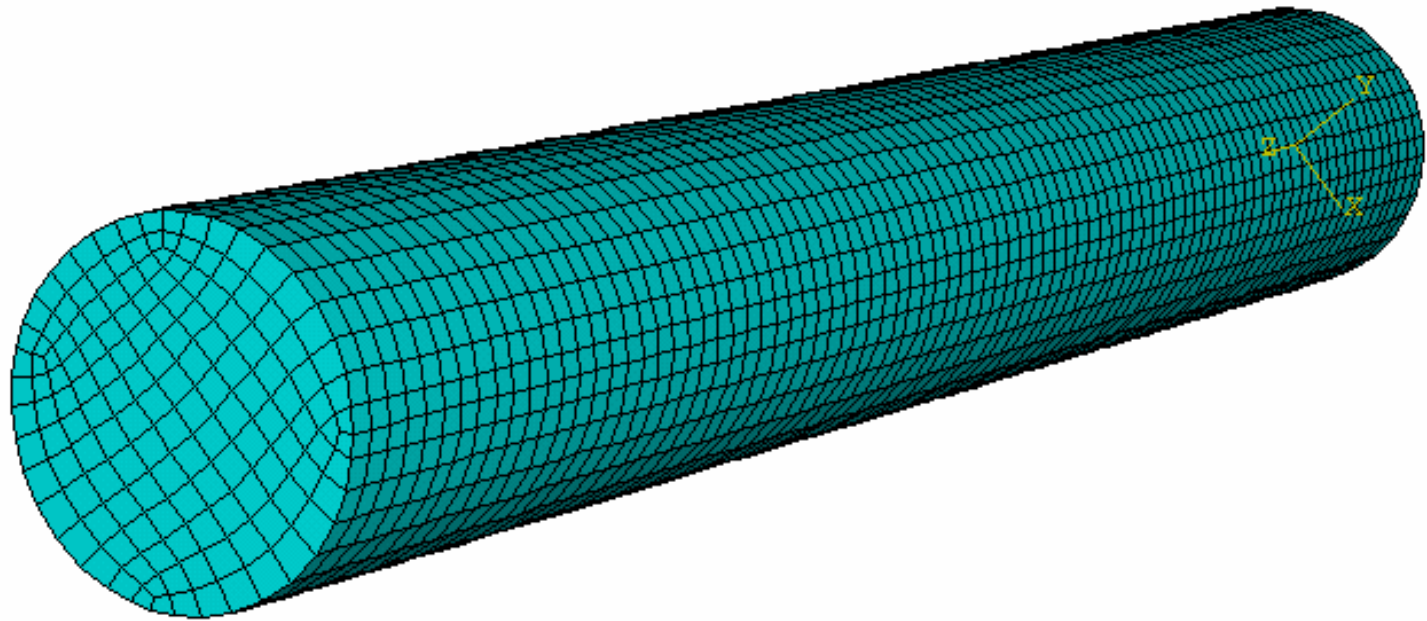


## Validation of Abaqus UMAT

---

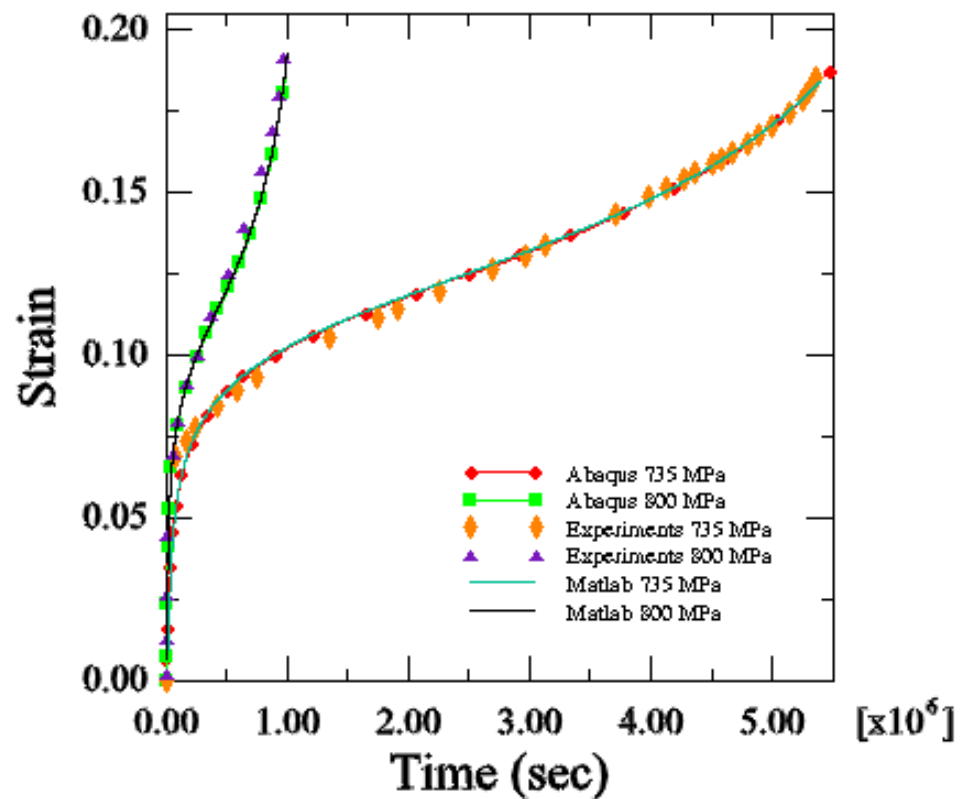
- The UMAT for our constitutive model has been validated by comparing results for cases with available experimental results
- Elaborate testing of the UMAT is done for a variety of cases to validate its efficacy

# Typical Finite Element Mesh

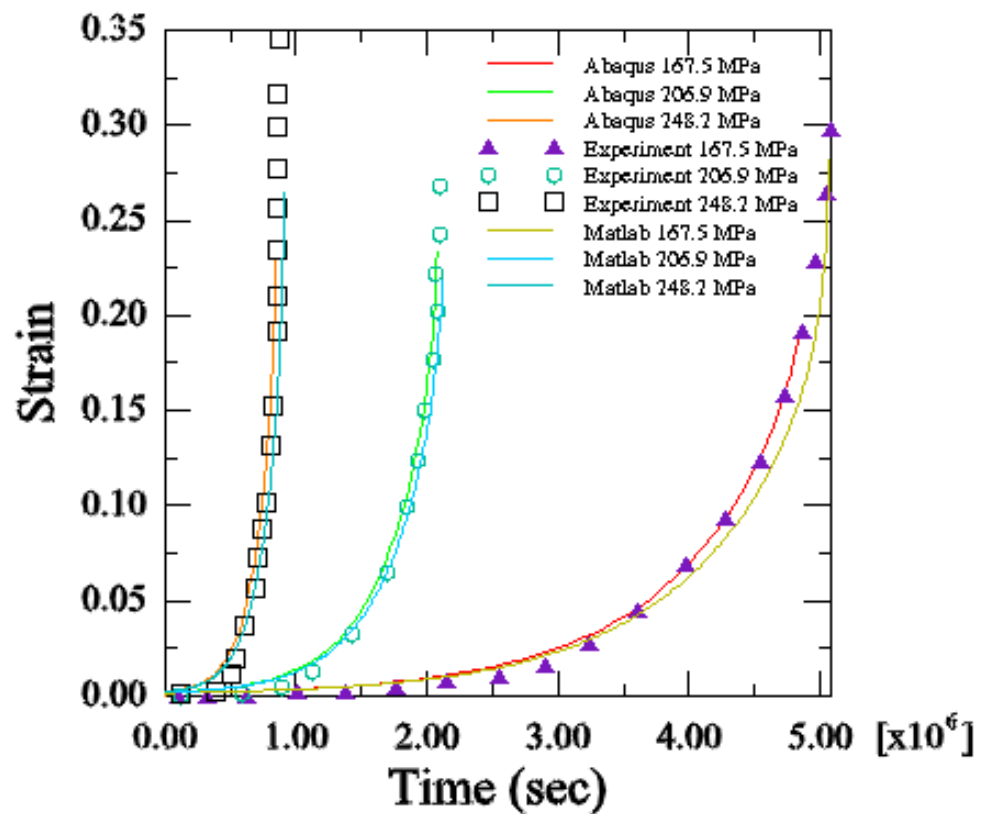




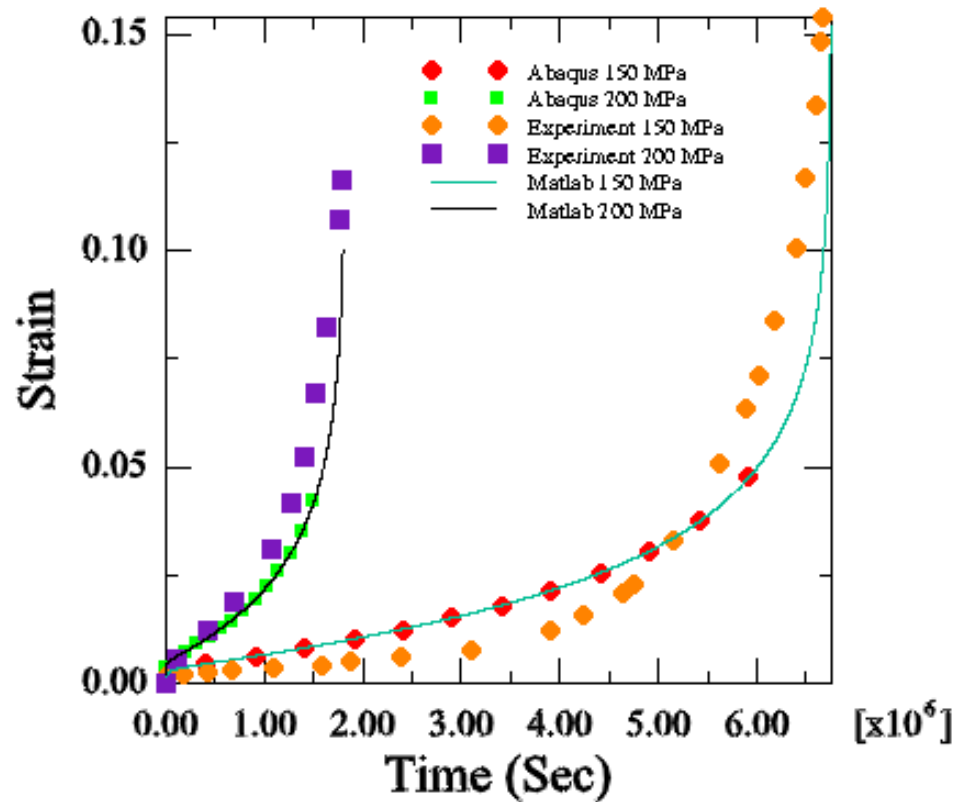
## Comparison of Results, Strain (CMSX-4 , 750 °C, <001>, Svoboda & Lucas (1998))



## Comparison of Results, Strain (CMSX-4, 982 °C, <001> Henderson & Lindblom (1997,))



## Comparison of Results (CMSX-4, <001>, 1000 °C, Svoboda & Lucas (1998),)





## Comparison of Results

---

- The model has been implemented in ABAQUS/STANDARD through User Defined Routines (UMAT, SDVINI, ORIENT)
- Experimental results, results obtained in MATLAB and results obtained in ABAQUS agree well
- First order implicit backward difference method implemented in UMAT is stable although time steps need to be controlled to achieve accurate results

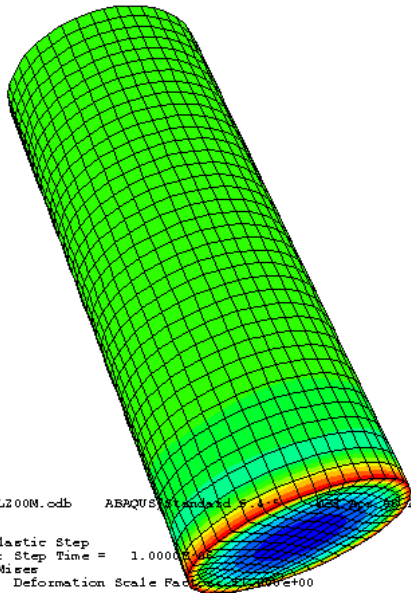
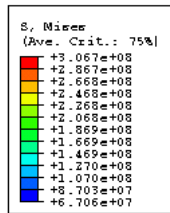
# Inhomogeneous Deformation of a $\langle 001 \rangle$ Oriented Creep Specimen

- UMAT is used to study inhomogeneous deformation of a creep specimen
- 800 °C,  $\langle 001 \rangle$  Oriented
- Boundary Conditions: Uniform tensile loading (200 MPa) along the top surface  
Bottom Plane is fixed in space

# Inhomogeneous Deformation of a $\langle 001 \rangle$ Oriented Creep Specimen

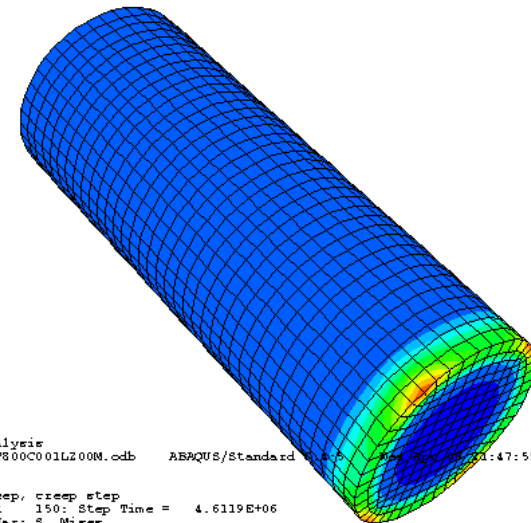
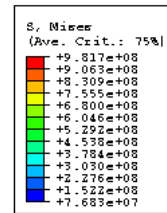
- Stresses after 1) initial elastic step  
2) after creep for 4.6E6 Secs (~1280 hours)

1)



3  
2  
1  
Creep Analysis  
JOB: InHT800C01L200M.cdb ABAQUS/Standard  
Step: Elastic, Elastic Step  
Increment 1: Step Time = 1.000E+00  
Primary Var: S, Mises  
Deformed Var: U Deformation Scale Factor: +1.000E+00  
21:47:59 CDT 2005

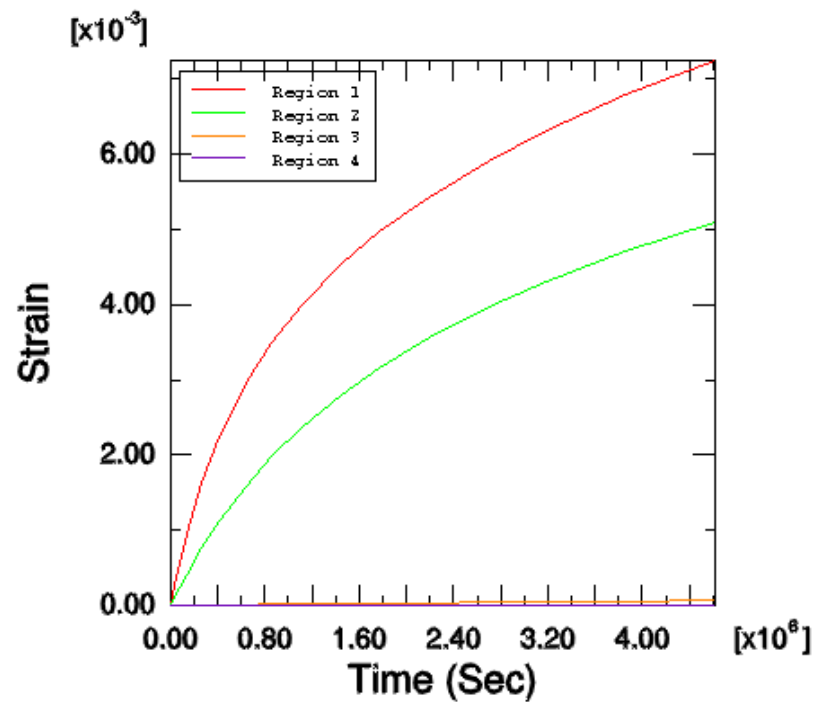
(2)



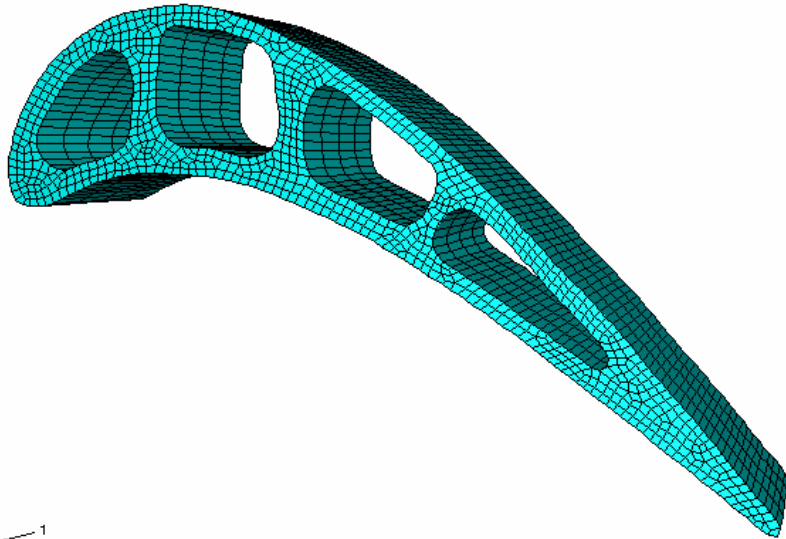
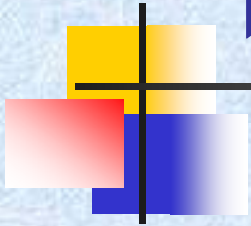
3  
2  
1  
Creep Analysis  
JOB: InHT800C01L200M.cdb ABAQUS/Standard  
Step: creep, creep step  
Increment 150: Step Time = 4.6119E+06  
Primary Var: S, Mises  
Deformed Var: U Deformation Scale Factor: +1.000E+00  
21:47:59 CDT 2005

# Inhomogeneous Deformation of a $\langle 001 \rangle$ Oriented Creep Specimen

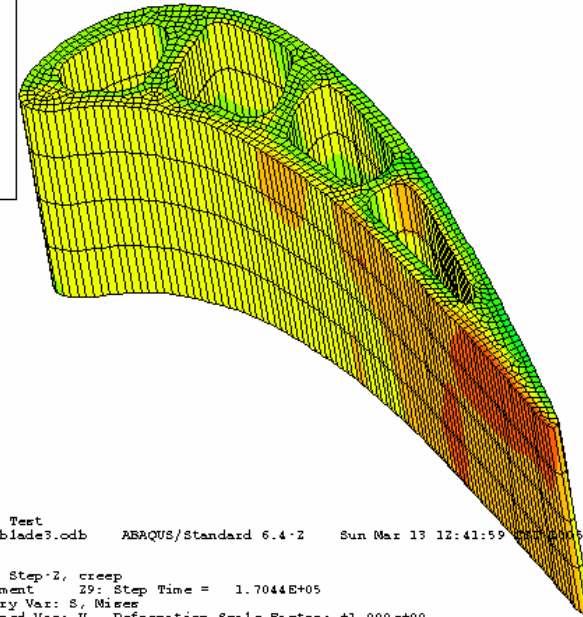
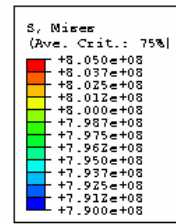
- Strain in various regions of stresses due to creep



# Homogeneous Deformation of Turbine blade



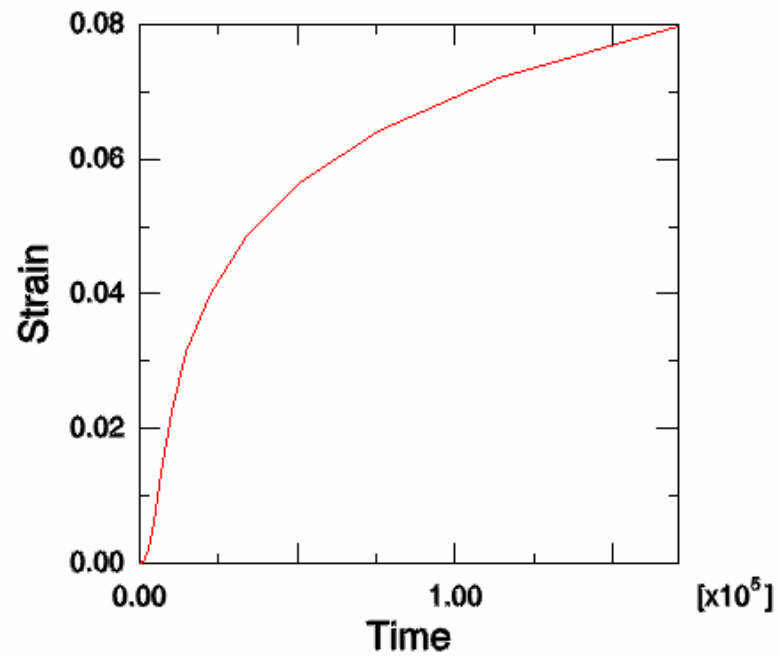
2  
3 1



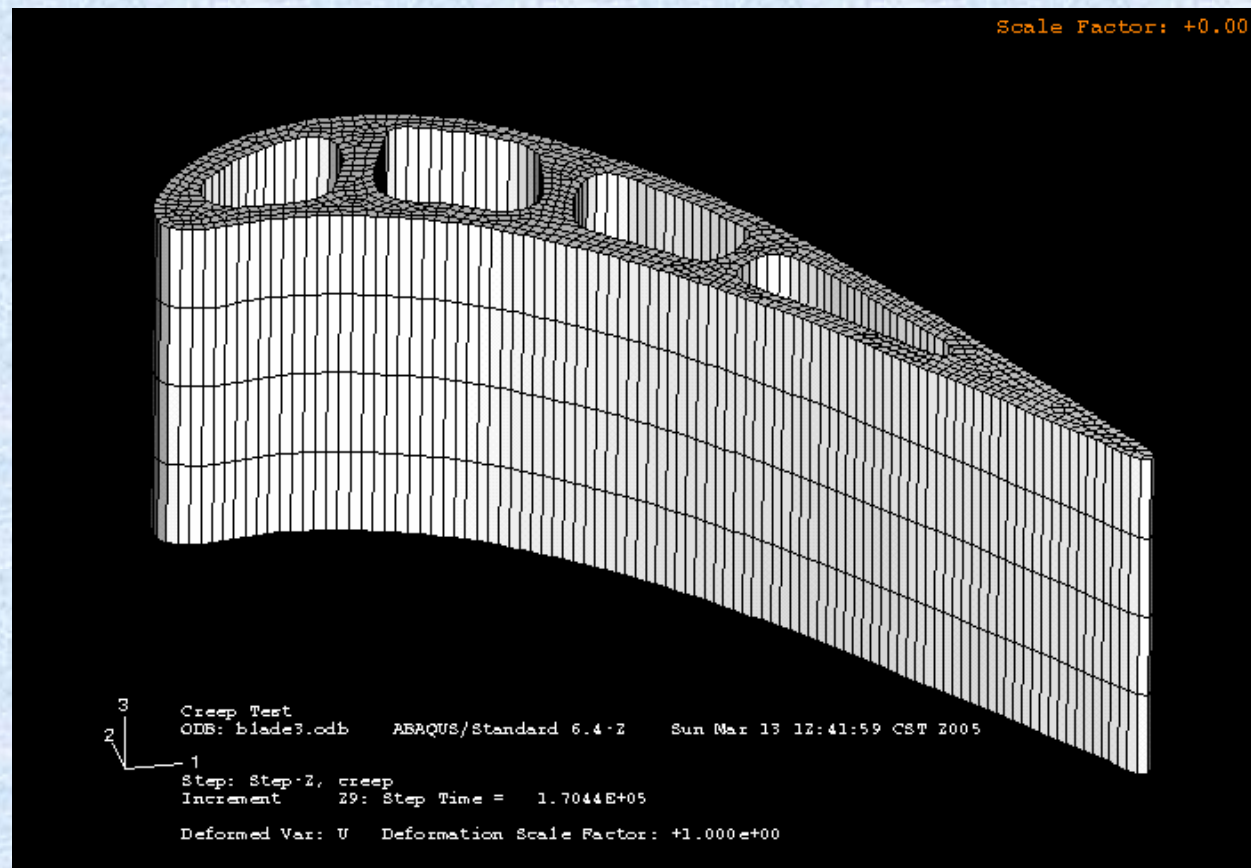
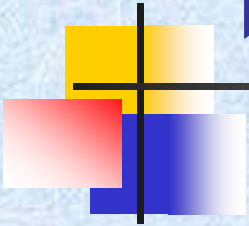
3 2  
1  
Creep Test  
ODB: blade3.cdb ABAQUS/Standard 6.4-2 Sun Mar 13 12:41:59  
Step: Step-2, creep  
Increment 29: Step Time = 1.7044E+05  
Primary Var: S, Mises  
Deformed Var: U Deformation Scale Factor: +1.000e+00



# Homogeneous Deformation of Turbine blade



# Homogeneous Deformation of Turbine blade



# Conclusion



---

- Development of constitutive model for creep has been successfully completed
- The model is successful in predicting creep behavior for
  - a range of temperatures pertinent to gas turbine blade applications (750 °C - 1000 °C)
  - a range of loads
  - loading in different orientations ( $\langle 001 \rangle$ ,  $\langle 111 \rangle$  and  $\langle 011 \rangle$ )

## Conclusion



---

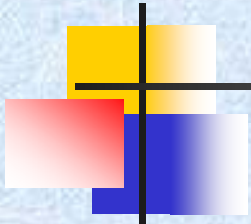
- The constitutive model has been implemented in Abaqus/Standard through UMAT
- The UMAT has been validated with experimental results and results for the case of a homogeneous deformation for loading along  $\langle 001 \rangle$
- The UMAT is able to solve for complex deformations

# Future Work



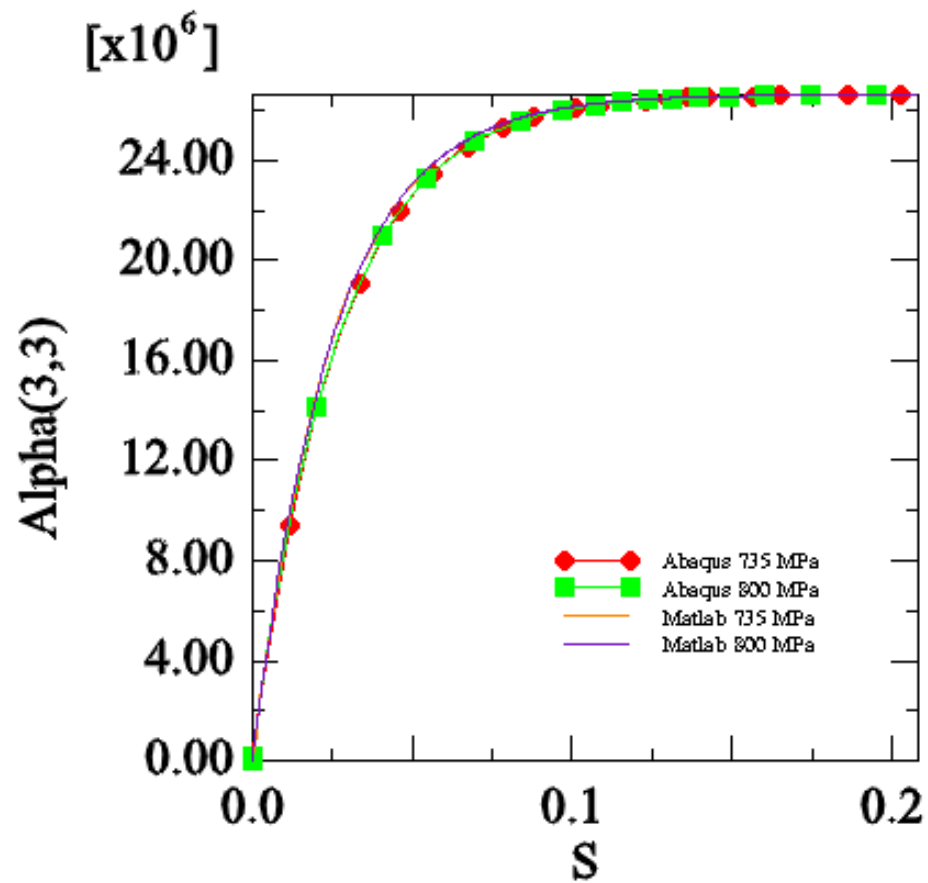
---

- Test UMAT for complex loading conditions in realistic geometries
- Optimize choice of stored energy, rate of entropy production to engineer specific properties

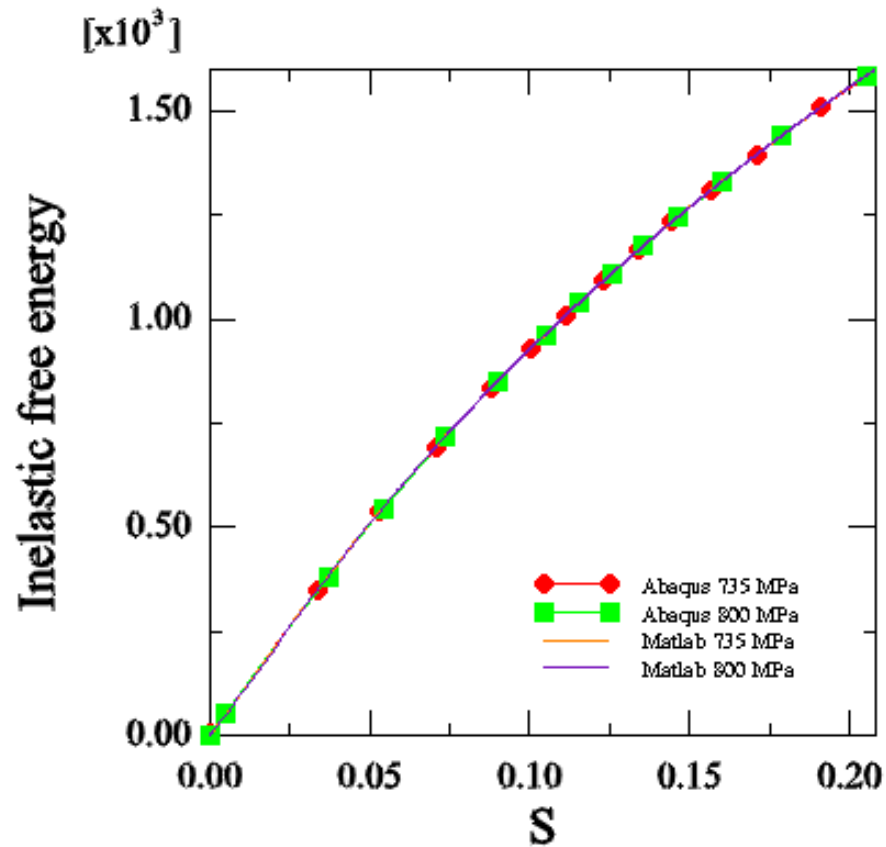


Thank You

# Comparison of Results, Backstress (CMSX-4, <001>, 750 °C, )

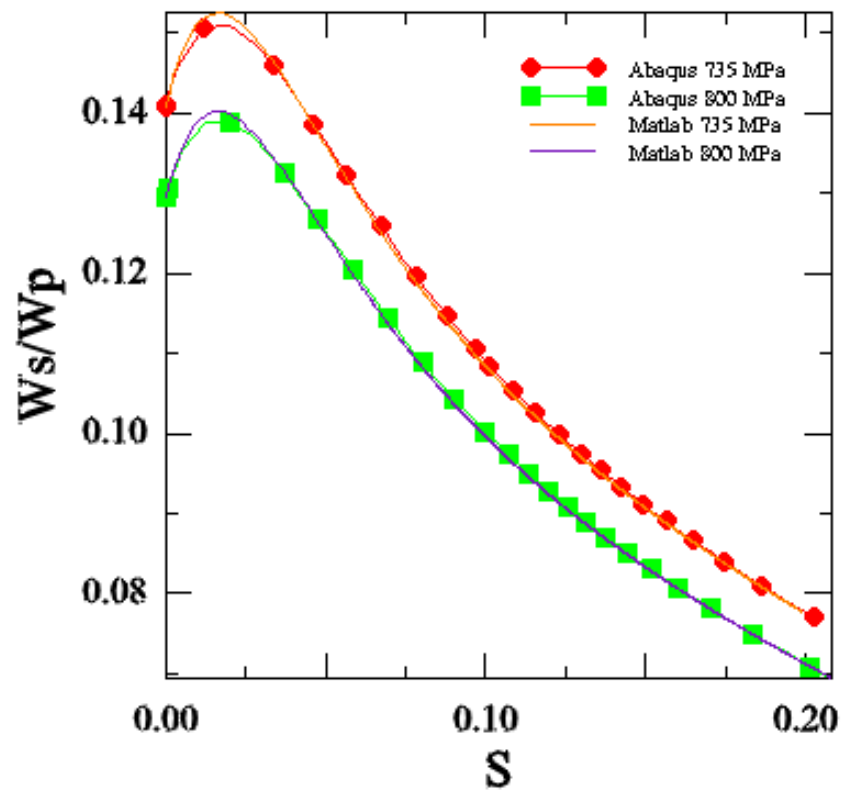


# Comparison of Results, Inelastic Stored Energy (CMSX-4, <001>, 750 °C)

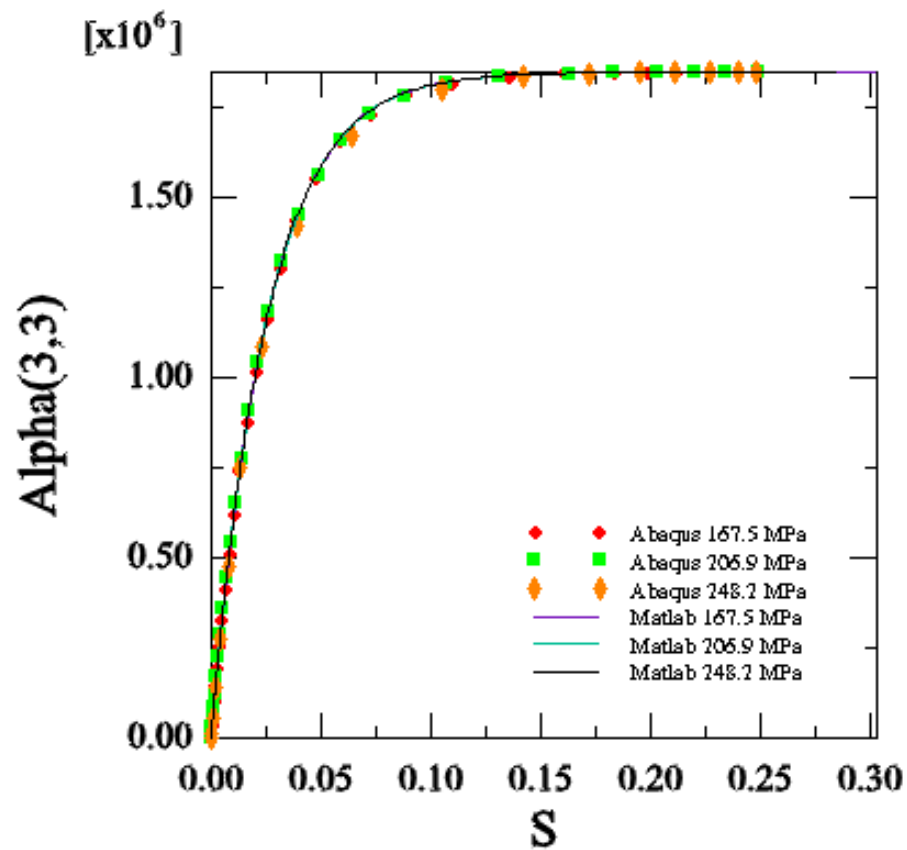




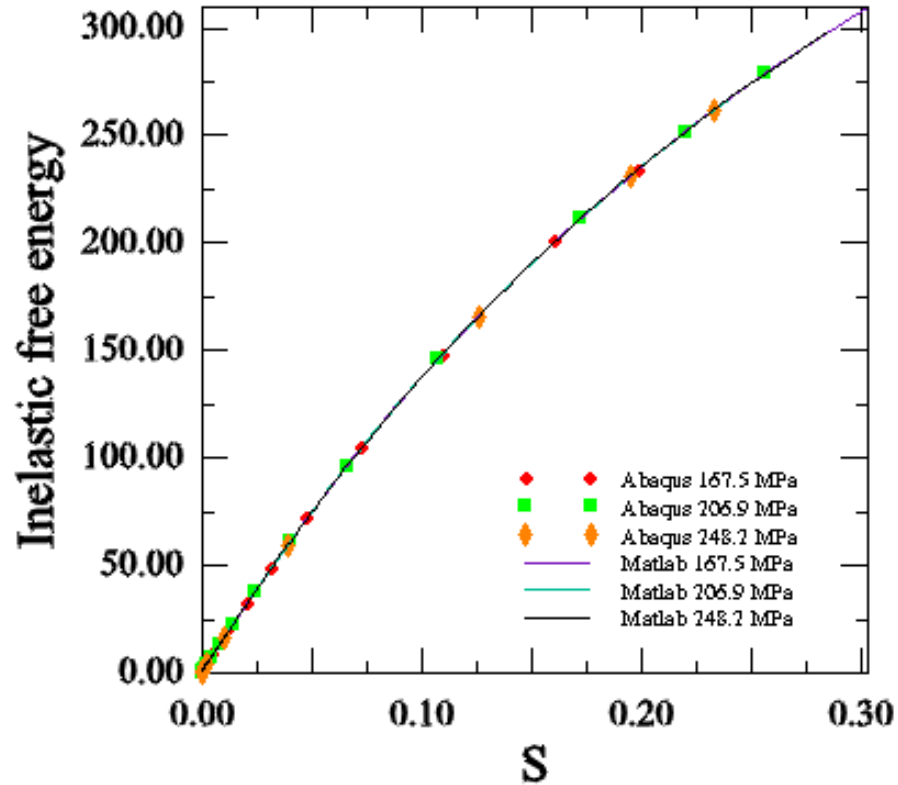
# Comparison of Results, $W_s/W_p$ (CMSX-4, $\langle 001 \rangle$ , 750 °C,)



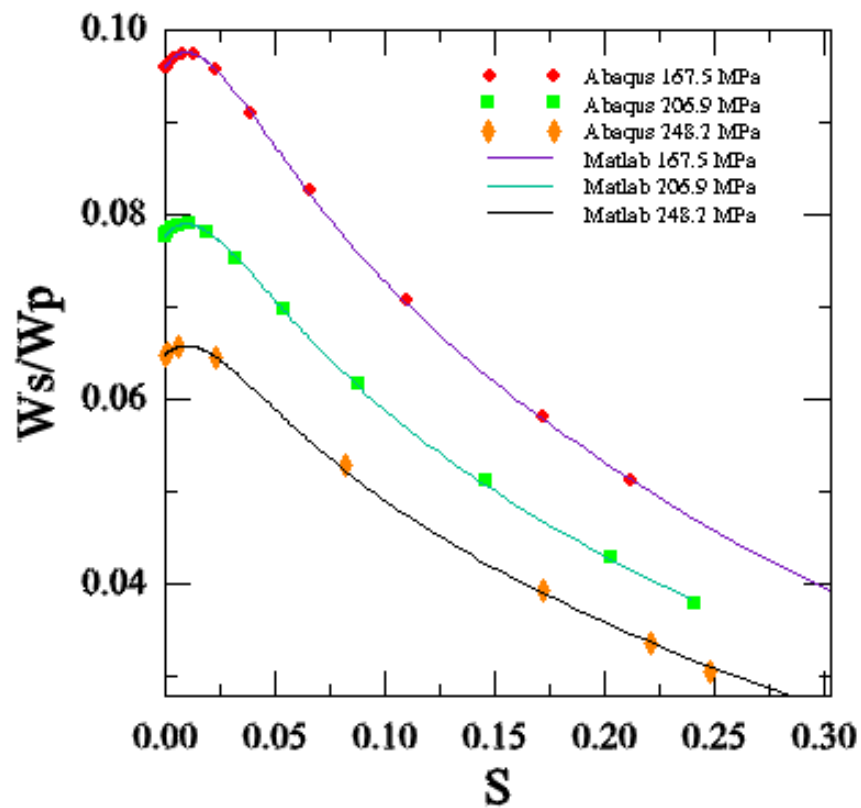
# Comparison of Results, Backstress (CMSX-4, <001>, 982 °C,)



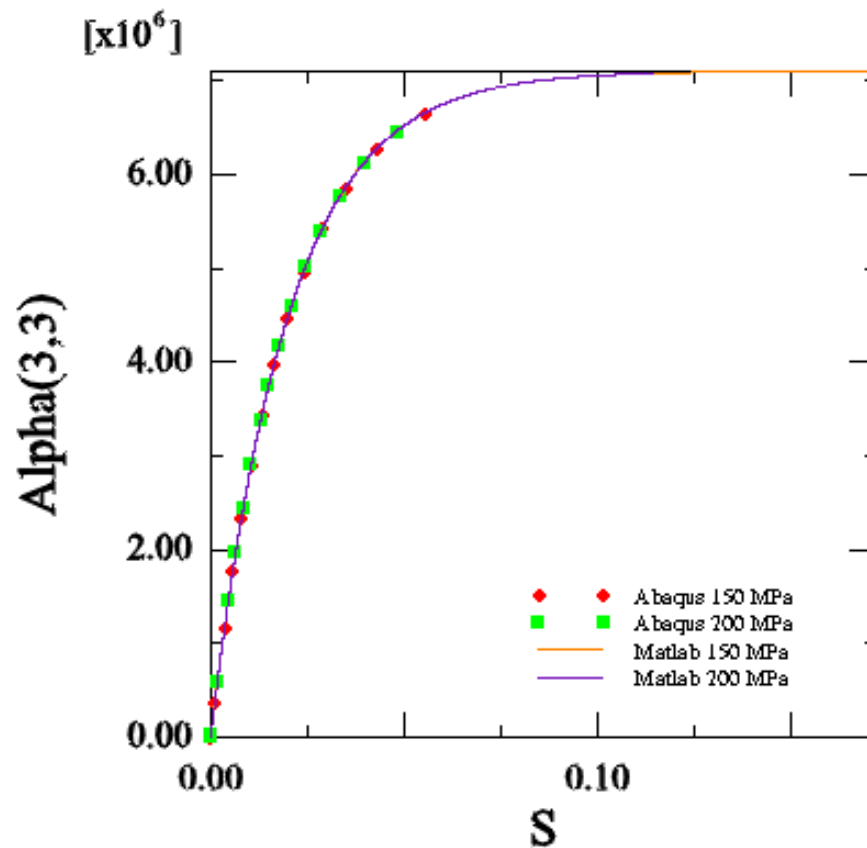
# Comparison of Results, Inelastic Stored Energy (CMSX-4, <001>, 982 °C)



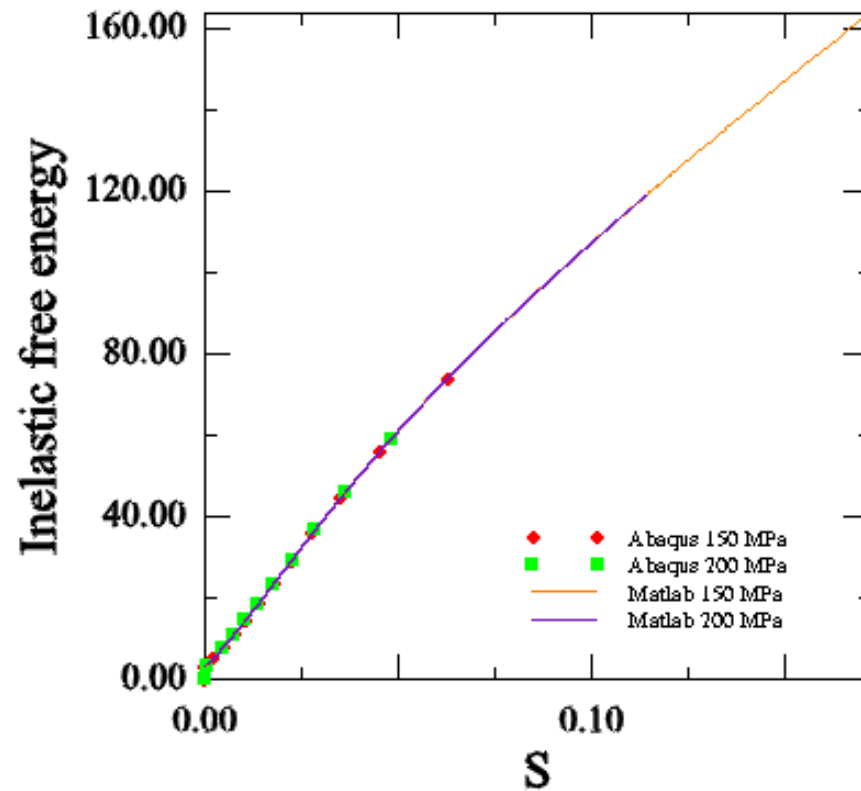
# Comparison of Results, $W_s/W_p$ (CMSX-4, $\langle 001 \rangle$ , 982 °C)



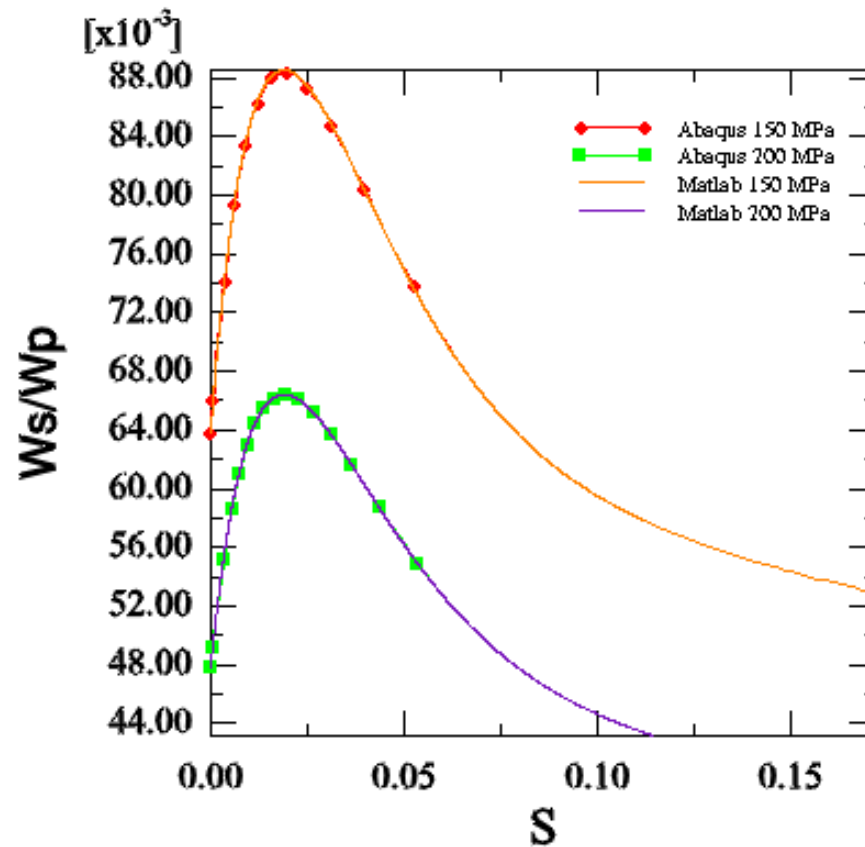
# Comparison of Results, Backstress (CMSX-4, <001>, 1000 °C,)



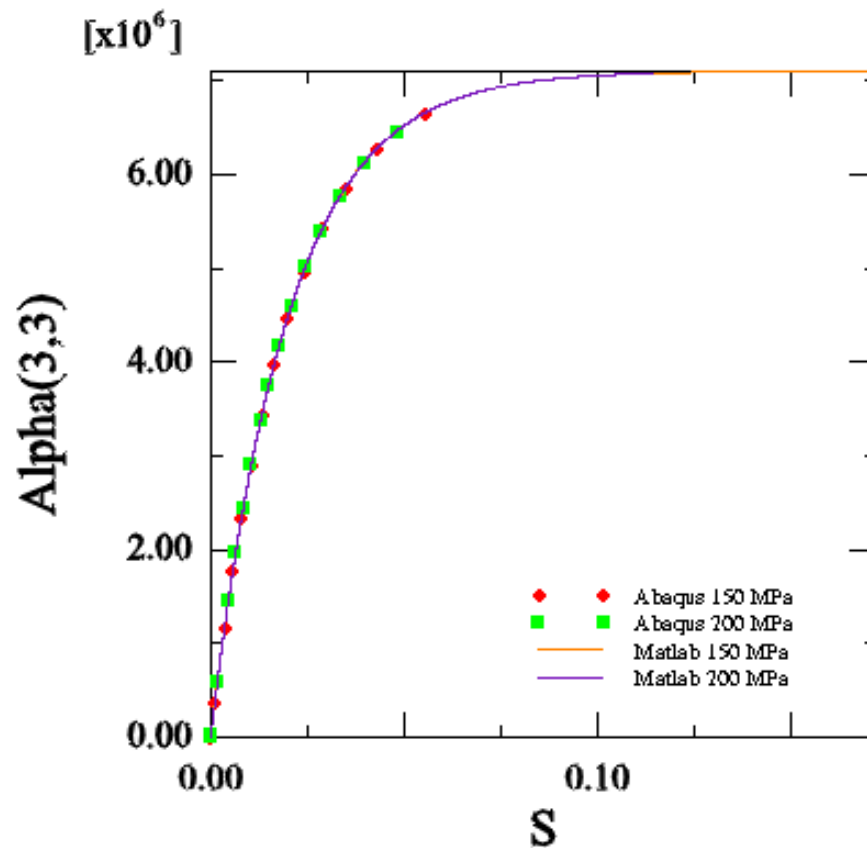
# Comparison of Results, Inelastic Stored Energy (CMSX-4, <001>, 1000 °C)



# Comparison of Results, $W_s/W_p$ (CMSX-4, $\langle 001 \rangle$ , 1000 °C,)

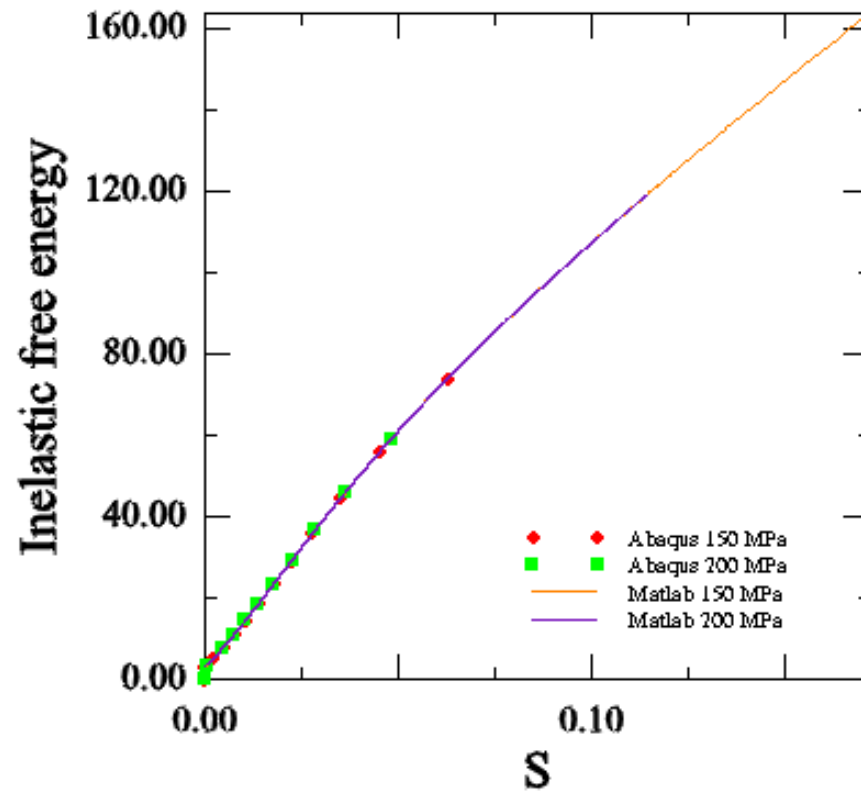


# Comparison of Results, Backstress (CMSX-4, <001>, 1000 °C,)

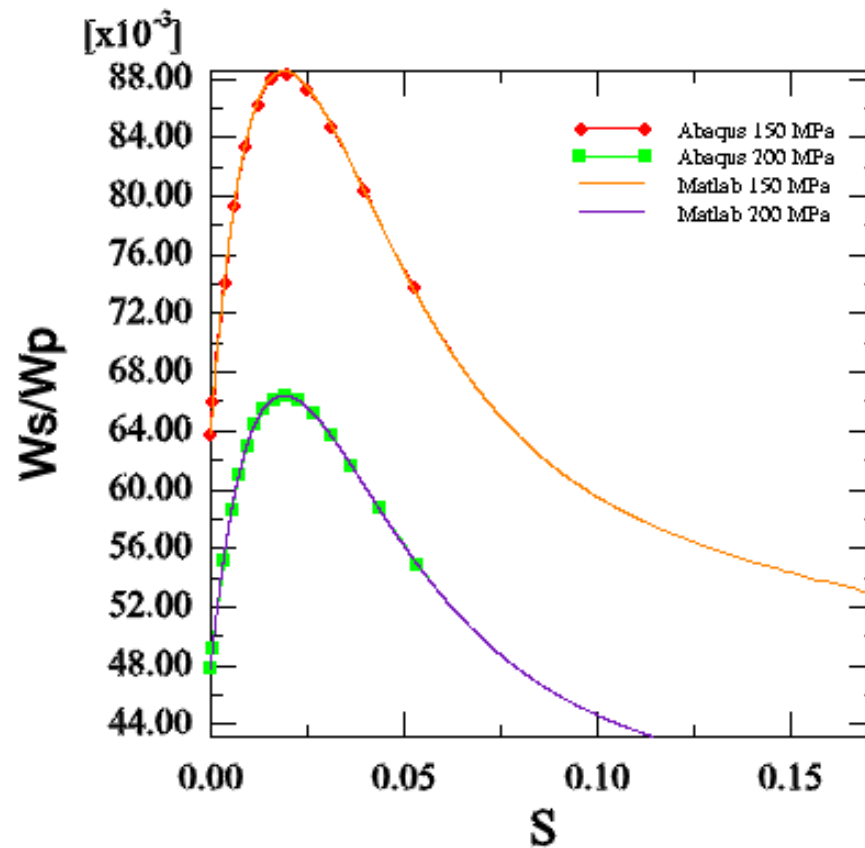




# Comparison of Results, Inelastic Stored Energy (CMSX-4, <001>, 1000 °C)



# Comparison of Results, $W_s/W_p$ (CMSX-4, $\langle 001 \rangle$ , 1000 °C,)





# Conclusion

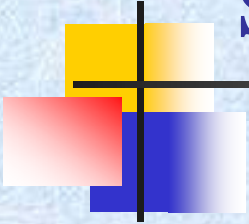
---

- The model is within a thermodynamic setting and takes into account the anisotropy associated with single crystal and its evolution with inelastic strain
- The model takes into account the microstructure of single crystal superalloys, motion of dislocations and their interaction with secondary precipitates

# Homogeneous Deformation of Turbine blade

- UMAT has been tested for Homogeneous deformation of a turbine blade at 800 °C,  $\langle 001 \rangle$  Oriented
- Boundary conditions: Uniform loading ( 800 MPa) on top surface,  
Bottom plane remain fixed in z direction (the direction of blade axis),  
One point on the bottom plane near the leading edge is fixed in space

# Typical Composition of Nickel Based Single Crystal Superalloys



	Ni	Cr	Co	Mo	W	Al	Ti	Ta	Re	Nb	V	Hf
First Generation												
Rene N4	62.6	9	8	2	6	3.7	4.2	4		0.5		
CMSX-2	66.6	8	4.6	0.6	7.9	5.6	0.9	5.8				
Second Generation												
Rene N5	61.8	7	8	2	5	6.2		7	3			0.2
CMSX-4	61.8	6.5	9	0.6	6	5.6	1	6.5	3			0.1
Third Generation												
Rene N6	57.4	4.2	12.5	1.4	6	5.75	0	7.2	5.4	0	0	0.15
CMSX-10	69.6	2	3	0.4	5	5.7	0.2	8	6	0.1		0.03